The Parkes multi-beam pulsar survey – I. Observing and data analysis systems, discovery and timing of 100 pulsars

R. N. Manchester,[1][★] A. G. Lyne,[2] F. Camilo,[2,3] J. F. Bell,[1] V. M. Kaspi,[4,5] N. D'Amico,[6,7] N. P. F. McKay,[2] F. Crawford,[5] I. H. Stairs,[2,8] A. Possenti,[6] M. Kramer[2] and D. C. Sheppard[2]

[1]*Australia Telescope National Facility, CSIRO, P.O. Box 76, Epping NSW 1710, Australia*
[2]*University of Manchester, Jodrell Bank Observatory, Macclesfield, Cheshire SK11 9DL*
[3]*Columbia Astrophysics Laboratory, Columbia University, 550 W. 120th Street, New York, NY 10027, USA*
[4]*McGill University, Ernest Rutherford Physics Building, 3600 University Street, Montreal, QC, H3A 2T8, Canada*
[5]*Massachusetts Institute of Technology, Center for Space Research, 70 Vassar Street, Cambridge, MA 02139, USA*
[6]*Osservatorio Astronomico di Bologna, via Ranzani 1, 40127 Bologna, Italy*
[7]*Istituto di Radioastronomia del CNR, via Gobetti 101, 40129 Bologna, Italy*
[8]*National Radio Astronomy Observatory, Green Bank, WV 24944, USA*

ABSTRACT

The Parkes multi-beam pulsar survey is a sensitive survey of a strip along the Galactic plane with $|b| < 5°$ and $l = 260°$ to $l = 50°$. It uses a 13-beam receiver on the 64-m Parkes radio telescope, receiving two polarizations per beam over a 288-MHz bandwidth centred on 1374 MHz. The receiver and data acquisition systems are described in some detail. For pulsar periods in the range 0.1–2 s and dispersion measures of less than $300 \, \mathrm{cm}^{-3}$ pc, the nominal limiting flux density of the survey is about 0.2 mJy. At shorter or longer periods or higher dispersions, the sensitivity is reduced. Timing observations are carried out for pulsars discovered in the survey for 12–18 months after confirmation to obtain accurate positions, spin parameters, dispersion measures, pulse shapes and mean flux densities. The survey is proving to be extremely successful, with more than 600 pulsars discovered so far. We expect that, when complete, this one survey will come close to finding as many pulsars as all previous pulsar surveys put together. The newly discovered pulsars tend to be young, distant and of high radio luminosity. They will form a valuable sample for studies of pulsar emission properties, the Galactic distribution and evolution of pulsars, and as probes of interstellar medium properties. This paper reports the timing and pulse shape parameters for the first 100 pulsars timed at Parkes, including three pulsars with periods of less than 100 ms which are members of binary systems. These results are briefly compared with the parameters of the previously known population.

Key words: methods: observational – pulsars: general.

1 INTRODUCTION

Since the discovery of pulsars more than 30 years ago (Hewish et al. 1968), many different searches for these objects have contributed to the 730 or so pulsars known prior to mid-1997 when the survey described here commenced. Some efforts with a relatively narrow focus have resulted in the discovery of extremely important objects, for example, the Crab pulsar (Staelin & Reifenstein 1968) or the first millisecond pulsar (Backer et al. 1982). However, the vast majority of known pulsars have been found in larger-scale searches. These searches generally have well-defined selection

criteria and hence provide samples of the Galactic population which can be modelled to determine the properties of the parent population. Most of our knowledge about the Galactic distribution and the evolution of pulsars has come from such studies (e.g. Lyne, Manchester & Taylor 1985; Lorimer et al. 1993; Hartman et al. 1997; Cordes & Chernoff 1998; Lyne et al. 1998). Of particular significance are young pulsars. These are often associated with supernova remnants (e.g. Kaspi 2000), show significant period irregularities such as glitches (Lyne, Shemar & Graham-Smith 2000) and have pulsed emission at optical, X-ray and γ-ray wavelengths (e.g. Wallace et al. 1977; Thompson et al. 1999).

Of comparable importance, however, are the serendipitous discovery of unusual and often unique objects by larger-scale

[★]E-mail: rmanches@atnf.csiro.au

surveys. Examples of this abound – for example, the first binary pulsar, PSR B1913+16 (Hulse & Taylor 1974), the first star with planetary-mass companions (Wolszczan & Frail 1992), the first pulsar with a massive stellar companion (Johnston et al. 1992b), and the first eclipsing pulsar (Fruchter, Stinebring & Taylor 1988). Pulsars show an amazingly diverse range of properties and most major surveys turn up at least one object with new and unexpected characteristics. Some of these are of great significance. The prime example is of course PSR B1913+16, which has provided the first observational evidence for gravitational waves and the best evidence so far that general relativity is an accurate description of gravity in the strong-field regime (Taylor & Weisberg 1989).

Pulsars are relatively weak radio sources. Successful pulsar surveys therefore require a large radio telescope, low-noise receivers, a relatively wide bandwidth and long observation times. Pulsar signals suffer dispersion because of the presence of charged particles in the interstellar medium. The dispersion delay across a bandwidth of $\Delta\nu$ centred at a frequency ν is

$$\tau_{DM} = 8.30 \times 10^3 \, DM \, \Delta\nu\nu^{-3} \, s, \tag{1}$$

where the dispersion measure, DM, is in units of $cm^{-3}\,pc$ and the frequencies are in MHz. To retain sensitivity, especially for short-period, high-dispersion pulsars, the observing bandwidth must be sub-divided into many channels. In most pulsar searches to date, this has been achieved using a filterbank system.

The sensitivity of pulsar searches is also limited by the Galactic radio continuum background and by interstellar scattering, especially for low radio frequencies and at low Galactic latitudes. Interstellar scattering results in a one-sided broadening of the observed pulse profile with a frequency dependence $\sim \nu^{-4.4}$ (e.g. Rickett 1977) which cannot be removed by using narrow bandwidths. Most pulsar searches along the Galactic plane have therefore been at higher radio frequencies, often around 1400 MHz (e.g. Clifton et al. 1992; Johnston et al. 1992a).

The Clifton et al. (1992) 1400-MHz survey was carried out using the 76-m Lovell Telescope at Jodrell Bank Observatory, and covered a strip along the Galactic plane with $|b| < 1.1°$ between longitudes of 355° and 95°, with a narrower extension to 105°. The limiting sensitivity to long-period pulsars away from the Galactic plane was about 1 mJy. A total of 61 pulsars was detected, of which 40 were not previously known. Johnston et al. (1992a) carried out a complementary survey of the southern Galactic plane in the region $|b| < 4°$ and between $l = 270°$ and $l = 20°$, with a central frequency of 1500 MHz. The limiting sensitivity was very similar to that for the Clifton et al. survey. A total of 100 pulsars was detected, of which 46 were previously unknown. These surveys found a sample of young and generally distant pulsars which are strongly concentrated at low Galactic longitudes, $|l| \lesssim 40°$. They include a number of interesting objects, including the eclipsing high-mass binary system PSR B1259 − 63 (Johnston et al. 1992b) and many glitching pulsars (Shemar & Lyne 1996; Wang et al. 2000).

The Parkes multi-beam receiver was conceived with the aim of undertaking large-scale and sensitive searches for relatively nearby galaxies ($z \lesssim 0.04$) by detection of their emission in the 21-cm line of neutral hydrogen. The receiver has 13 feeds with a central feed surrounded by two rings, each of six feeds, arranged in a hexagonal pattern (Staveley-Smith et al. 1996). This arrangement permits the simultaneous observation of 13 regions of sky, increasing the speed of surveys by approximately the same factor. It was quickly realized that this system would make a powerful instrument for pulsar surveys, provided the bandwidth was increased above the original specification and the necessary large filterbank system could be constructed. A new data acquisition system capable of handling multi-beam data sets was also a fundamental component of the system.

These requirements were met, and the Parkes multi-beam pulsar survey commenced in 1997 August. This survey aims to cover a strip with $|b| < 5°$ along the Galactic plane between Galactic longitudes of 260° and 50°. The filterbank system gives 96×3 MHz channels of polarization-summed data for each beam which are sampled every 250 μs. Observation times per pointing are 35 min, giving a very high sensitivity, about seven times better than those of the Clifton et al. (1992) and Johnston et al. (1992a) surveys, at least for pulsars not in short-period binary systems. Although not yet complete, the survey has been outstandingly successful, with over 600 pulsars discovered so far.

Preliminary reports on the multi-beam survey and its results have been given by Camilo et al. (2000a); Manchester et al. (2000); Lyne et al. (2000); D'Amico et al. (2000). Also, papers on the discovery of several pulsars of particular interest have been published. Lyne et al. (2000) announced the discovery of PSR J1811–1736, a pulsar with a period of 104 ms in a highly eccentric orbit of a period of 18.8 d with a companion of minimum mass $0.7\,M_\odot$, most probably a neutron star, making this the fourth or fifth double neutron star system known in the Galactic disc. Camilo et al. (2000b) report the discovery of two young pulsars, J1119–6127 and J1814–1744, which have the highest surface dipole magnetic field strengths among known radio pulsars. PSR J1119–6127 has a characteristic age, τ_c, of only 1600 yr, a measured braking index, $n = 2.91 \pm 0.05$, and is associated with a previously unknown supernova remnant (Crawford et al. 2001; Pivovaroff et al. 2001). PSR J1814–1744 has a much longer period, 3.975 s, and the highest inferred surface dipole field strength of any known radio pulsar, 5.5×10^{13} G, in the region of so-called 'magnetars' (Pivovaroff, Kaspi & Camilo 2000). PSR J1141–6545 is a relatively young pulsar ($\tau_c \sim 1.4$ Myr) in an eccentric 5-h orbit for which the relativistic precession of periastron has been measured (Kaspi et al. 2000). This implies that the total mass of the system is $2.30\,M_\odot$, indicating that the companion is probably a massive white dwarf formed before the neutron star we observe as the pulsar. Stairs et al. (2001) discuss the high-mass binary system PSR J1740–3052, which is in a highly eccentric 230-d orbit with a companion star of minimum mass $11\,M_\odot$. A possible companion is a late-type star identified on infrared images, but the absence of the expected eclipses and precession of periastron caused by tidal interactions suggest that the actual companion may be a main-sequence B-star or a black hole hidden by the late-type star. Camilo et al. (2001) report the discovery of five circular-orbit binary systems with orbital periods in the range 1.3–15 d. Three of these pulsars, PSRs J1232–6501, J1435–6100 and J1454–5846, as well as PSR J1119 − 6127, were discovered early in the survey and hence are included in the pulsars described in this paper. Finally, D'Amico et al. (2001) report the discovery of two young pulsars, PSRs J1420–6048 and J1837–0604, which may be associated with EGRET γ-ray sources.

In the following section we describe the observing and analysis systems and the search strategy. Timing observations undertaken after the confirmation of a pulsar and our data release policy are described in Section 3. In Section 4, we give parameters for the first 100 pulsars discovered by the survey. Implications of these results are discussed in Section 5. Detailed information about the survey,

observing instructions, data release policy, and results may be found under the pulsar multi-beam web page.[1]

2 OBSERVING AND SEARCH ANALYSIS SYSTEMS

In this section, we describe in detail the receiver system, data acquisition system, analysis procedures and search strategy being used for the Parkes multi-beam pulsar survey.

2.1 The receiver system

The Parkes multi-beam receiver consists of a 13-feed system operating at a central frequency of 1374 MHz, with a bandwidth of 288 MHz at the prime focus of the Parkes 64-m radio telescope. Orthogonal linear polarizations are received from each feed and fed to cryogenically cooled HEMT amplifiers, constructed under contract at Jodrell Bank Observatory. The horns are arranged in a double hexagon around a central horn with a spacing between horns of 1.2 wavelengths; the corresponding beam spacing on the sky is close to twice the nominal half-power beamwidth of 14.2 arcmin (Staveley-Smith et al. 1996). Measured system parameters[2] are listed in Table 1. System temperatures vary by a degree or so over the 26 receivers; the value of 21 K quoted in the table is an average value. For the central beam, this corresponds to an equivalent system flux density of 28.6 Jy. Outer feeds have a somewhat lower efficiency, reduced by about 0.27 db for the inner ring and 1.0 db for the outer ring. The outer beams are also somewhat elliptical, with the major axis in the radial direction, and have a significant coma lobe. Predicted beam patterns for the central and outer beams are given by Staveley-Smith et al. (1996); at least to the half-power point, the beam patterns are well represented by a two-dimensional Gaussian function.

After further amplification, all 26 signals are down-converted in the focus cabin to intermediate frequency using a local oscillator frequency of 1582 MHz. These signals are transferred to the tower receiver room via low-loss coaxial cables and pass through cable-equalising amplifiers and level setting attenuators to a down-conversion system. This splits the 288-MHz bandwidth of each signal into three equal parts with output between 64 and 160 MHz using an up-down conversion system with band-limiting filters centred at 1060 MHz. These signals are then fed to a very large filterbank system, designed and constructed at Jodrell Bank Observatory and Osservatorio Astronomico di Bologna, which gives 96 3-MHz channels for each polarization of each feed. The output of each filter is detected and summed with its corresponding polarization pair. These summed outputs are high-pass filtered with an effective time constant of approximately 0.9 s, integrated for the sampling interval of 250 μs and then one-bit digitised.

2.2 Data acquisition and analysis

Data acquisition is controlled by a multi-threaded C++ program, PMDAQ, running on a Digital Alpha PICMG processor. A custom-designed board with a programmable Xilinx device is installed on the computer's PCI bus, and interfaces between the digitizer and an Ikon-10116 16-bit direct memory access card. Integration of the first sample of an observation is triggered by the Observatory 1-s

---

[1] http://www.atnf.csiro.au/research/pulsar/pmsurv/.
[2] From http://www.atnf.csiro.au/research/multi-beam/lstavele/description.html.

pulse, allowing measurement of pulse arrival times. The first 16-bit word of every input sample is a counter which is checked by the data acquisition program and then discarded. Time synchronization is further checked by using a 5-s pulse from the Observatory clock. Data can be output to disc, double-density Exabytes and digital linear tapes (DLTs). Each output block contains a 640-B header giving telescope, receiver, source and observation parameters and 48 kB of one-bit data, all from a single beam. Successive blocks have data from successive beams. Survey-mode data are normally output to DLTs and timing data to Exabytes. For survey observations, the data rate is $640\,\mathrm{kB\,s^{-1}}$, which fills a DLT in approximately 15 hr of continuous observation.

Observations are controlled using a Tcl–Tk interface to a control program, PMCTRL, operating on a Sun Sparc workstation. The interface allows setting of observation parameters such as the receiver, filterbank system, sampling interval, observation time, output device, pointing centre and feed position angle, and the logging of operator messages. PMCTRL has socket interfaces to the Observatory clock, the telescope drive system and the receiver translator system and a remote procedure call (RPC) interface to PMDAQ. The program maintains a record of tape operations and handles status returns and error conditions from the telescope or data acquisition system. It also writes a summary observation file and a complete log file giving details of all observations. Details of the observing strategy for the multi-beam survey are given in Section 2.4.

Observations can be monitored in real time using a program, PMMON, which runs on a networked workstation with user input via a Tcl–Tk interface. PMMON communicates with PMDAQ via an RPC interface, obtaining either complete tape blocks or data streams summed across all filter channels for each beam. Several forms of output are provided, including mean digitizer levels for each beam, modulation spectra and time sequences for each beam, and modulation spectra for each filterbank channel of a given beam. The latter form of output is especially valuable for tracing narrow-band interference. For observations of known pulsars (normally with the centre beam), integrated pulse profiles for each frequency channel and a dedispersed mean pulse profile can be displayed and may be recorded to disc for later examination.

Offline processing runs on networked workstations at each of the collaborating institutions under the control of a JAVA program, PMPROC. The processing consists of four main stages. Data are first examined for the presence of narrow-band radio-frequency interference by computing the modulation spectrum for each frequency channel, normally using a subset of each data file of length 2^{19} samples. Samples in channels containing strong interference are set to zero or one in alternate channels (to give a mean of 0.5) as the data are transferred to disc in subsequent stages.

The second stage of processing concerns identification of interfering signals in the modulation spectrum. As most interference is undispersed, this analysis is performed on the 'zero-DM' spectrum. Data for each observation are summed across all frequency channels on reading from the tape to produce a zero-DM data stream of 2^{23} samples per beam. This is Fourier-transformed to give the modulation spectrum. Known signals which are present all or most of the time, such as the power line frequency (50 Hz) and its harmonics, are first identified and their bandwidth determined. The remaining spectrum is then searched for significant spectral features. This search is performed on the fundamental spectrum and on spectra obtained by summing 2, 4, 8 and 16 harmonics. The signals are identified and their bandwidth and harmonic content recorded. Any signal which appears in four

Table 1. Feed and receiver parameters.

	Centre	Inner Ring	Outer Ring
Number of beams	13		
Polarizations/beam	2		
Frequency channels/polarization	96×3 MHz		
System temperature (K)	21		
Beam	Centre	Inner Ring	Outer Ring
Telescope gain (K/Jy)	0.735	0.690	0.581
Half-power beamwidth (arcmin)	14.0	14.1	14.5
Beam ellipticity	0.0	0.03	0.06
Coma lobe (db)	none	-17	-14

or more beams of a given pointing is flagged as interference; that signal and its harmonics are deleted in subsequent processing steps for that pointing. Similarly, any signal which appears in a given beam in more than three pointings is marked for deletion in subsequent processing for that beam in all pointings on that tape, and any signal which appears more than seven times in any beam of a given tape is marked for deletion in all pointings on that tape. A summary output is produced for each tape (normally containing 20–25 pointings) which gives grey-scale images of the modulation spectra as a function of beam and pointing, and lists the frequency ranges identified as interference.

In the third and major stage of processing, the data are searched for periodic signals over a range of dispersion delays. The basic analysis procedure is very similar to that employed in the Parkes Southern pulsar survey and described in detail by Manchester et al. (1996). A 'tree' dedispersion algorithm (Taylor 1974) is used. Dispersion delays are proportional to ν^{-2}, but the tree algorithm assumes that they are linear with frequency. This is approximately true for small fractional bandwidths, but the multi-beam survey has a fractional bandwidth of about 20 per cent, and straightforward application of tree dedispersion would lead to excessive pulse smearing for short-period pulsars. Also, the tree algorithm requires the number of frequency channels to be a power of two. To overcome these problems, the delays are 'linearized' on reading from tape. The number of frequency channels is increased from 96 to 128, and channel data streams are reassigned in channel number to remove the second-order dispersion-delay term. These channel reassignments are independent of dispersion measure.

The linearized data are split into eight sub-bands, each band consisting of 16 channels. A tree dedispersion is performed on each of these sub-bands to give dedispersed data streams for 16 dispersions between zero and the 'diagonal DM' (at which the dispersion smearing across one channel equals the sampling interval), approximately 35 cm^{-3} pc. These are subsequently added with varying delays to give a range of DMs about the central value. Another application of the tree algorithm to delayed data gives a further 16 data streams for dispersions from 35 to 70 cm^{-3} pc. Data samples are then summed in pairs to give an effective sampling interval of 0.5 ms and the tree algorithm is applied again to give 16 data streams for dispersions from 70 to 139 cm^{-3} pc. This process is repeated up to four more times, to an effective sampling interval of 8 ms, until a maximum DM of either 2177 cm^{-3} pc or 42/sin|b| cm^{-3} pc (where b is the Galactic latitude), whichever is less, is reached. The dedispersed data streams for each sub-band are then summed with a range of delays to give up to 325 dedispersed data streams with DM in the range 0 to 2203 cm^{-3} pc. The DM steps are 0.54 cm^{-3} pc for the first tree data set, 0.81 cm^{-3} pc for the second, and 26 cm^{-3} pc for the last, increasing by roughly a factor of two for each successive tree data set after the second.
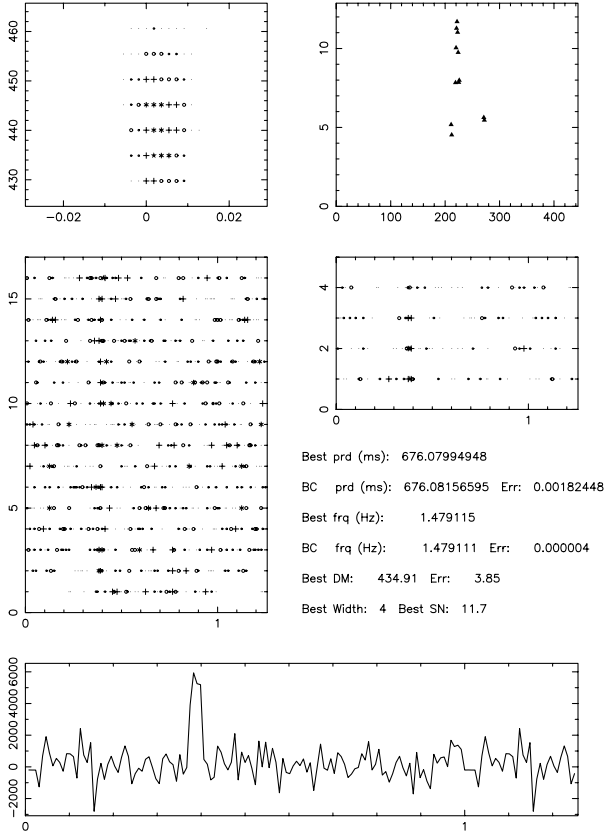
For each DM, the summed data stream is high-pass filtered by subtracting a running mean of length 2.048 s and then Fourier-transformed using a fast Fourier transform (FFT) routine. After deletion of spectral channels affected by interference and interpolation to recover spectral features lying mid-way between Fourier bins, the resulting spectra are searched for significant peaks. This process is repeated for spectra in which 2, 4, 8 and 16 harmonics have been summed to give a set of 50 candidate periods (10 from the fundamental and 10 from each harmonic sum) for each DM. A pulse profile is then formed for each candidate period by inverse transformation of the complex Fourier components for the fundamental and its harmonics, and the signal-to-noise ratio of this profile is computed. All such profiles from the full analysis over all DMs for a given beam are then ordered by signal-to-noise ratio. For the top 66 candidates, the appropriate tree data streams are summed into four sub-bands and folded into 16 sub-integrations, each of duration a little over 2 min, using the nominal period and DM. These are then summed with a range of delays in frequency and time, up to one sample per sub-band and per sub-integration, respectively, to search for the highest signal-to-noise ratio over a range of period and DM about the nominal values. The candidate parameters, including the maximum signal-to-noise ratios obtained from the harmonic summing, the reconstructed profile and results from the P–DM search are then recorded for later examination.

In the next stage of processing, candidates from all pointings on a given tape are collated and searched for common periods. Candidate periods seen in more than 6 beams are rejected as interference. Remaining candidates with a P–DM signal-to-noise ratio above a threshold (normally 8.0, corresponding to a random occurrence every few beams) are then examined using an interactive display and classified as Class 1 or Class 2 candidates or rejected as probable interference. Fig. 1 shows the display plot for a typical Class 1 candidate, later confirmed as a pulsar. The classification is necessarily somewhat subjective and is based on the similarity of the subplots to those for known pulsars. The most important criteria are final signal-to-noise ratio, continuity across sub-integrations and sub-bands of the pulse signal, and a well-defined peak in signal-to-noise ratio versus DM. The signal should also be linear or parabolic (indicating a constant acceleration) in the phase–time plot and linear in the phase–frequency plot. Most Class 1 candidates have a signal-to-noise ratio of 10 or more. For the early low-latitude phases of the survey, a Class 1 candidate was selected every one or two pointings. Each candidate is identified by a unique code based on the processing centre and a sequential number.

Candidates are then re-observed using the centre beam of the multi-beam receiver in order to confirm their reality as pulsars. Observations are made at five grid positions, the nominal position and four positions offset in latitude and longitude by 9 arcmin,

File: PM0068_037A%46905111 RAJ: 10:56:13.3 DecJ: −57:10:58. Gl: 287.783 Gb: 2.261 Date:
Centre freq. (Hz): 1.47911900 Centre period (ms): 676.07812500 Centre DM: 445.18
File start (blks): 1 Spectral s/n: 6.2 Recon s/n: 13.6 Blk length (s) 0.76800 L
Tsamp (ms): 2.0000 Frch1: 1516.5000 DM factor: 1.0 Sus: A0181 Class:1
Ref MJD: 51101.85745 BC Ref MJD: 51101.85419

Best prd (ms): 676.07994948

BC prd (ms): 676.08156595 Err: 0.00182448

Best frq (Hz): 1.479115

BC frq (Hz): 1.479111 Err: 0.000004

Best DM: 434.91 Err: 3.85

Best Width: 4 Best SN: 11.7

Figure 1. Display plot for typical candidate, later confirmed as a pulsar, PSR J1056–5709. Clockwise from the top left, the sub-plots show a crude grey-scale of the dependence of signal-to-noise ratio on dedispersion DM and offset (in ms) from the nominal period, the dependence of signal-to-noise ratio on DM trial number, a greyscale plot of signal-to-noise ratio versus pulse phase for four sub-bands across the observed bandwidth of 288 MHz, the final mean pulse profile, and a greyscale plot of signal-to-noise ratio versus pulse phase for successive sub-integrations, each of approximately 2 min duration.

normally with 6 min integration per point. These observations are searched in period and DM about the nominal values and, if two or three detections are obtained, an improved position is computed from the relative signal-to-noise ratio. If there is no detection in the grid observations, a 35-min observation is made at the nominal position and searched for a significant signal. This search is usually made using Fourier techniques to detect pulsars whose period may have changed significantly from the nominal value, caused by, for example, binary motion. Candidates which are not re-detected in one or two such observations are down-graded or rejected. To date, all Class 1 candidates have been re-observed with about 80 per cent of them being confirmed as pulsars.

2.3 Survey sensitivity

Survey parameters are summarized in Table 2. The system sensitivity for the centre beam has been modelled by Crawford (2000), assuming the parameters given in Tables 1 and 2. The raw

limiting flux density is given by the radiometer equation

$$S_{\lim} = \frac{\sigma \beta T_{\text{sys}}}{G \sqrt{B N_{\text{p}} \tau_{\text{obs}}}} \tag{2}$$

where σ is a loss factor, taken to be 1.5,[3] β is the detection signal-to-noise ratio threshold, taken to be 8.0, T_{sys} is the system temperature, G is the telescope gain, B is the receiver bandwidth in Hz, N_{p} is the number of polarizations and τ_{obs} is the time per observation in seconds.

An idealized pulse train of frequency $f_1 = P^{-1}$, where P is the pulse period, is represented in the Fourier domain by its fundamental and 15 harmonics $F(f_i)$, where each of the harmonics has an amplitude $y_0(f_i) = 1/S_{\lim}$. These harmonics are then multiplied by a series of functions, representing the responses of the various filters in the system, to give a final set of Fourier amplitudes $y(f_i)$. The first filter function is the Fourier transform of the intrinsic pulse profile, assumed to be Gaussian with a half-power width of $W_{50} = 0.05P$,

$$|g_1(f)| = \exp\left(-\frac{\pi^2 f^2 W_{50}^2}{4 \ln 2}\right) \tag{3}$$

and by a similar function $g_2(f)$ representing the Fourier transform of the smearing caused by dispersion in each filter channel, also assumed to have a Gaussian response, with W_{50} replaced by τ_{DM} (equation 1). As the analysis is based on the amplitude spectrum and each of the filters is real, we only have to consider the amplitude response of each filter.

The harmonics are then multiplied by the Fourier response of each of the filters in the hardware and software system. These result from the finite sampling interval,

$$|g_3(f)| = \left|\frac{\sin(\pi f \tau_{\text{samp}})}{\pi f \tau_{\text{samp}}}\right|, \tag{4}$$

the digitizer high-pass filtering, a two-pole filter with amplitude response

$$|g_4(f)| = \frac{(2\pi f \tau_{\text{HP}})^2}{[1 + (2\pi f \tau_{\text{HP}})^4]^{1/2}}, \tag{5}$$

where $\tau_{\text{HP}} = 0.9$ s (see Section 4), and a software high-pass filter, implemented by subtracting a box-car average of length $\tau_S = 2.048$ s from the dedispersed data stream, giving

$$|g_5(f)| = 1 - \frac{\sin(\pi f \tau_S)}{\pi f \tau_S}. \tag{6}$$

Table 2. Pulsar multi-beam survey parameters.

Galactic longitude range	260° to 50°
Galactic latitude range	−5° to 5°
Hexagonal grid spacing	0°.2333
Number of survey pointings	2670
Sampling interval, τ_{samp}	250 μs
Observation time/pointing, τ_{obs}	2100 s
Limiting sensitivity for centre beam	0.14 mJy

---

[3] One-bit sampling at the Nyquist rate introduces a loss of $\sqrt{2/\pi}$ relative to a fully sampled signal (cf. Van Vleck & Middleton 1966). The principal remaining loss results from the non-rectangular bandpass of the channel filters.
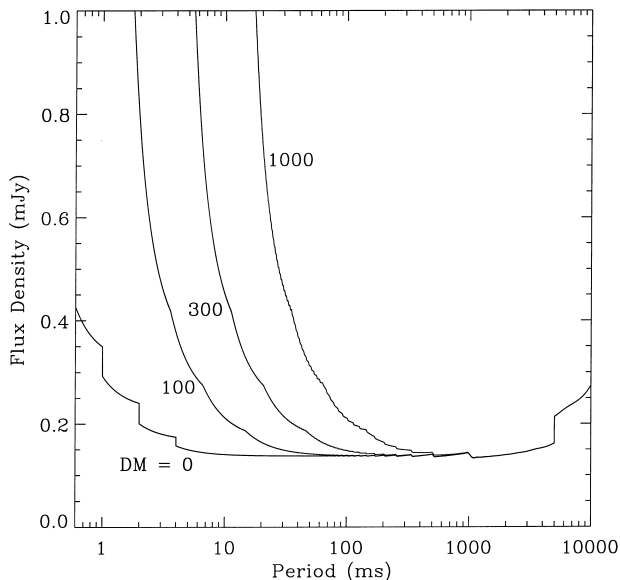
Figure 2. Minimum detectable flux density for the Parkes multi-beam survey as a function of pulsar period and DM. These calculations refer to the centre of the central beam of the multi-beam system, are for an assumed pulse width of $0.05P$ and do not include the effects of increased system temperature due to the Galactic sky background emission or the effects of interstellar scattering or interference.

The harmonic range is then limited to $f > f_{\min}$, where $f_{\min} = 0.2\,\text{Hz}$, a limit set mainly by the need to reject low-level interference and other red noise, and $f < f_N = 1/(2\tau_{\text{samp}})$, the Nyquist frequency. Harmonics of the lowest valid signal frequency are then summed to give a final amplitude

$$Y(f_n) = \frac{\sum_{i=1}^{n} y(f_i)}{\sqrt{n}}. \tag{7}$$

The final limiting sensitivity $S_{\min}$ is then given by

$$S_{\min} = \frac{1}{Y_{\max}(f_n)}, \tag{8}$$

where $Y_{\max}(f_n)$ is the largest $Y(f_n)$ for $n = 1, 2, 4, 8$ or 16.

The resultant sensitivity curves for four representative values of DM are shown in Fig. 2. These curves show that for low-DM pulsars with periods greater than about 10 ms, the limiting sensitivity is about 0.14 mJy. Steps in the zero-DM curve at short periods result from changes in the number of harmonics below the Nyquist frequency; at higher DMs, the higher harmonics are attenuated and the steps are not as evident. Steps between 100 ms and 1 s result from the software high-pass filtering. The Fourier cut-off at $f_{\min}$ and the hardware and software high-pass filtering results in reduced sensitivity at longer periods.

Especially for distant pulsars near the Galactic plane, the sensitivity is degraded by two effects not included in the modeling: sky background temperature (T_{sky}) and pulse smearing due to scattering (τ_{scatt}). Limiting sensitivities should be scaled by factors $(T_{sys} + T_{\text{sky}})/T_{sys}$ and $[w/(P - w)]^{1/2}/[w_0/(P - w_0)]^{1/2}$, where $w = (W_{50}^2 + \tau_{samp}^2 + \tau_{\text{DM}}^2 + \tau_{\text{scatt}}^2)^{1/2}$ is the effective pulse width, W_{50} is the intrinsic pulse width, and $w_0 = [(0.05P)^2 + \tau_{samp}^2 + \tau_{\text{DM}}^2]^{1/2}$. Sky background temperatures are highest close to the Galactic plane and towards the Galactic Centre; for example at $(l, b = 300°, 0°)$, $T_{\text{sky}} \sim 5\,\text{K}$, and for

$(l, b = 350°, 0°)$, $T_{\text{sky}} \sim 18\,\text{K}$. Scattering parameters have not yet been measured for the multi-beam pulsars, but a cursory examination of the mean pulse profiles shows that at least 15 per cent have scattering broadening of a few milliseconds or more.

It should also be emphasized that these sensitivity figures refer to centre of the central beam. As Table 1 shows, the outer beams are less sensitive. Averaged over the 13 beams, the limiting sensitivity is about 0.16 mJy. Also, of course, pulsars do not usually lie at the beam centre in the discovery observation. The limiting sensitivity is further degraded by the beam response at the position of the pulsar relative to that at the beam centre. The average beam gain over the hexagonal area covered by one beam (see Section 2.4 below) assuming a gaussian beamshape, is 0.70, giving an average limiting flux density for the survey as a whole of 0.22 mJy.

The sensitivity is also degraded by radio frequency interference, but this is much more difficult to quantify. There are many forms of interference, including both natural and man-made signals. Natural interference such as lightning is not a major problem as it is not periodic and some protection is afforded by the one-bit digitization. Some of the man-made interference originates from within the Observatory and even from within the receiving system itself, but most sources are narrow-band transmissions such as radar beacons and communication links. Much of the interference is transient, which makes it difficult to trace. Typically six–eight frequency channels are routinely rejected because they contain persistent modulated narrow-band signals. The sensitivity of the system to modulation at the power-line frequency (50 Hz) was minimized by choosing a sampling interval such that the Nyquist frequency is a harmonic of 50 Hz. Although not strictly interference, beam 8A has been disconnected since the start of the survey because of a quasi-periodic gain modulation occurring in the cryogenically cooled part of the receiver. Also, coupling within the one-bit digitizer results in periodic signals at frequencies of $f_N/2^n$, where n is an integer, and their harmonics. These are rejected in the Fourier domain. After rejection of the known sources of interference, typically there are 20–30 narrow-band signals ('birdies') detected in the zero-DM modulation spectra for a full tape. These are flagged and deleted from the pointings in which they were detected. Typically, much less than one per cent of the modulation spectrum is rejected.

2.4   Search strategy

The 13 beams of the multi-beam receiver are spaced by approximately two beamwidths on the sky. Therefore interleaved pointings are required to cover a given region. As shown in Fig. 3, a cluster of four pointings covers a region about 1.5° across, with adjacent beams touching at the half-power points. The clusters tessellate to fully cover a region. For this configuration, the multi-beam receiver must be oriented at a Galactic position angle of 30°. As the time per pointing is relatively long (35 min), the variation of parallactic angle is tracked during the observation. The range of parallactic angle is ±180° but the multi-beam receiver has a feed-angle range limited to ±75°, and so ±60° or ±120° may be added to the feed angle to keep it within the legal range throughout the observation. This changes the labels on the beams in Fig. 3 but not the pattern.

The survey region, $-100° < l < 50°$ and $|b| < 5°$, is covered by a grid of survey pointings, defined by

$$l = (i_l - 5000 + 0.5i_{b2})d_l \tag{9}$$
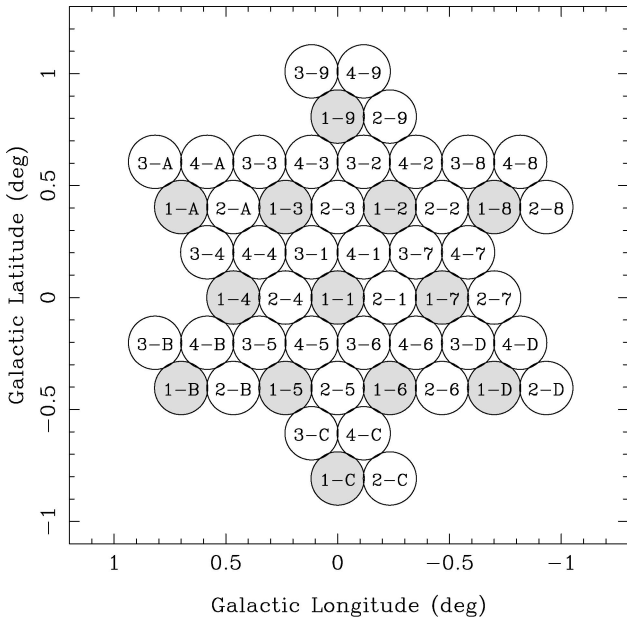
Figure 3. Beam locations for a cluster of four pointings for a feed Galactic position angle of 30°. Beams are labeled with a pointing number within the cluster and the hexadecimal beam number; beams for pointing 1 are shaded.

and

$$b = (i_b - 500)d_b, \tag{10}$$

where

$$i_l = 4400 + 7n + 2m + c_l, \tag{11}$$

$$i_b = 500 - 2n - 8m + c_b, \tag{12}$$

$d_l = 0.5\Delta$, $d_b = 0.5\Delta \sin 60°$, $\Delta = 0°.46667$ is the beam separation, and i_{b2} is 1 if i_b is odd and 0 if i_b is even. The pointings within a cluster are defined by $(c_l, c_b) = (0, 0)$, $(1, 0)$, $(0, 1)$ and $(-1, 1)$, and n and m are integers, the range of which is determined by the area to be covered. For example, the pointing closest to the Galactic Centre is at $l = 359°.767$, $b = 0°.0$, with $i_l = 4999$ and $i_b = 500$, corresponding to $n = 92$, $m = -23$ and $(c_l, c_b) = (1, 0)$.

A record of the observational and processing status is maintained in a file, where each pointing is identified by a seven-digit number, $1000i_l + i_b$, known as the pointing ID. The inverse transformation, from (l, b) to the nearest pointing ID is given by

$$i_b = 500 + b/d_b + 0.5 \tag{13}$$

and

$$i_l = 5000 + l/d_l - 0.5i_{b2} + 0.5, \tag{14}$$

where $-180° < l \leq 180°$. Each of the 13 beam positions has a unique 'grid ID' which, for a feed Galactic position angle of 30°, is offset from the pointing ID by $\Delta i_l = 0, -1, 1, 2, 1, -1, -2, -3, 0, 3, 3, 0$ and -3, and $\Delta i_b = 0, 2, 2, 0, -2, -2, 0, 2, 4, 2, -2, -4$ and -2 respectively.

An interactive program, HEXVIEW, is used to display the status of each pointing and to select pointings for observation. Consecutive pointings observed in one session are separated by about 5° to avoid the possibility of a strong pulsar appearing in more than one pointing and hence possibly being flagged as interference. As a

system check, the strong pulsar PSR J1359–6038 is observed on most observing days for about 1 min, centred on each beam in turn.

Initially the survey region extended from $l = 220°$. However, a decision was made to limit it at $l = 260°$ after a few months because of the low pulsar density between these two longitudes. Observations began at low latitudes where the pulsar concentration is high. The discovery rate for the first year of observation was at the unprecedented rate of more than one pulsar per hour of observing time.

3 TIMING OBSERVATIONS AND ANALYSIS

Almost all follow-up investigations require a more precise pulsar position, pulsar period P, and/or period derivative $\dot{P}$ than those obtained from the discovery observation. Improved estimates of the DM, the mean pulsed flux density S_{1400} and the pulse widths at the 50 and 10 per cent levels, W_{50} and W_{10}, are also valuable. All of these parameters are determined from a series of timing observations made over a span of at least one year. These observations also reveal binary motion if present, and enable the binary parameters to be determined.

Timing observations are made using either the Parkes 64-m telescope or the Lovell 76-m telescope at Jodrell Bank Observatory, with most of the detected pulsars north of declination $-35°$ being timed at Jodrell Bank. In this paper, we give results only from Parkes timing observations. The centre beam of the multi-beam receiver is used, with the same filterbank and data acquisition system as is used for the survey. Typically, observations are of duration between 2 and 30 min, dependent upon the pulsar flux density, and are made at intervals of 2–6 weeks, with some more closely spaced observations to resolve pulse counting ambiguities.

The data for each observation are dedispersed and synchronously folded at the predicted topocentric pulsar period in off-line processing to form an 'archive' file. These files normally have eight sub-bands across the observed bandwidth and a series of sub-integrations, typically of 1-min duration. These are summed over both frequency and time to form a mean pulse profile. This is then convolved with a 'standard profile' for the corresponding pulsar, producing a topocentric time-of-arrival (TOA). These are then processed using the TEMPO program[4] which converts them to barycentric TOAs at infinite frequency and performs a multi-parameter fit for the pulsar parameters. Barycentric corrections are obtained using the Jet Propulsion Laboratory DE200 solar-system ephemeris (Standish 1990). Initially, standard profiles are formed from a high signal-to-noise ratio observation. Once a valid timing solution is obtained, all or most of the observations are summed to form a 'grand average' profile. A new standard profile is then made from this average profile and the TOAs recomputed. This often reduces the final residuals for the timing solution by a factor of two or more.

As evidenced by the discovery that PSR J2144–3933 has an 8.5-s period (Young, Manchester & Johnston 1999), standard search software can sometimes mis-identify the pulse period by a factor of two or three. As mentioned above (Section 2.3) there is a software limit at a period of 5 s. Furthermore, interference can sometimes mask low-frequency spectral components. In such cases a pulsar may be detected by its 2nd or 3rd harmonic, leading to the assumption of an incorrect period. Such errors can be identified by

[4] See http://pulsar.princeton.edu/tempo or http://www.atnf.csiro.au/research/pulsar/timing/tempo.

folding the data at twice and three times the nominal period and examining the resulting mean pulse profiles. This check is routinely done for all pulsars discovered in this survey and has resulted in period correction for several pulsars.

In a few pulsars, at the confirmation stage or soon after, significant variations in solar-system barycentric period are observed. These may be caused by an especially large period derivative, or to binary motion. In either case, an improved estimate of the barycentric period is obtained by summing the archive sub-integrations over a range of periods about the nominal value. Where the rate of period change is not too great, improved periods can be obtained by fitting TOAs for several observations over one or a few adjacent days. A series of these barycentric periods can then be fitted with either a period derivative term or a binary model. The parameters from this fit then form the basis for a coherent timing solution using TEMPO.

Improved estimates of the dispersion measure can also be obtained from individual archive files by summing the sub-bands with a range of delays corresponding to different DM values about the nominal value and searching for the highest signal-to-noise ratio. After a timing solution is available, a final DM value for each pulsar is obtained by summing each archive in time and forming four sub-bands across the 288-MHz observed bandwidth. TOAs are then obtained for all archives for each of the four sub-bands. Improved estimates of the DM and its error are then obtained using TEMPO, holding all parameters except DM fixed at the values from the final timing solution.

The grand average profile for each pulsar is also used as a basis for estimating the mean flux density and pulse width parameters. Flux densities were calibrated by observing a sample of 13 pulsars with previously catalogued 1400-MHz flux densities of moderate value (to give reasonable signal-to-noise ratio while avoiding digitizer saturation) and high DMs (to minimize variations caused by scintillation). Table 3 lists the pulsars used, their DM and their assumed flux density (Taylor, Manchester & Lyne 1993). This calibration is based on the accumulated digitizer counts with the multi-beam system, and hence is relative to the system equivalent flux density. The effect of the varying sky background temperature was allowed for in the calculation by scaling values of sky background temperature at 408 MHz from the Haslam et al. (1982) all-sky survey to 1374 MHz, assuming a spectral index of -2.5. Based on the rms fluctuation of computed flux densities among the calibration pulsars and independently calibrated observations of

these and other pulsars using the Australia Telescope Compact Array and the Caltech correlator (Navarro et al. 1997), we estimate that the flux scale is accurate at the 10–15 per cent level.

Except for a few especially interesting cases, timing observations cease 12–18 months after confirmation. By this time a coherent timing solution has normally been obtained, giving an accurate pulsar position, pulse period, period derivative, dispersion measure and, if applicable, binary parameters. Pulsars are renamed at this stage, based on the accurate J2000 position. The parameters are then entered into the pulsar catalogue, allowing accurate predictions for future observations, and listed on the Parkes multi-beam pulsar survey 'New Pulsars' web page.[5] The multi-beam pulsar survey web pages also specify policy for release of raw data tapes. On request, these are made available for copying two years after the date of recording. The 'Data Release' web page[5] lists all available observations sorted by date, Parkes project identification, observed position and tape label. We will provide documentation specifying the data format and software to read and copy data tapes on request.

4   DISCOVERY AND TIMING OF THE FIRST 100 PULSARS

In this paper we report the discovery of 100 pulsars by the Parkes multi-beam pulsar survey. These pulsars were selected as the first 100 from the list of pulsars being timed at Parkes, ordered by the date at which regular Parkes timing observations commenced. All are south of declination $-35°$. Table 4 lists the pulsar name, the J2000 right ascension and declination from the timing solution, the corresponding Galactic coordinates, the beam in which the pulsar was detected, the radial distance of the pulsar from the beam centre in units of the beam radius (cf. Table 1), the signal-to-noise ratio of the discovery observation from the final time-domain folding in the search process, the mean flux density averaged over all observations included in the timing solution, and pulse widths at 50 and 10 per cent of the peak of the mean pulse profile. Flux densities have been corrected for off-centre pointing during the timing observations. Many of these pulsars were detected more than once by the survey. Beam and signal-to-noise (S/N) details refer to the detection having the highest signal-to-noise ratio. The 10 per cent width is not measurable for pulsars with mean profiles having poor signal-to-noise ratio. Estimated uncertainties are given in parentheses where relevant and refer to the last quoted digit. Flux densities may be somewhat over-estimated for very weak pulsars or those which have extended null periods, because non-detections are not included in the timing solution.

Table 5 gives solar-system barycentric pulse periods, period derivatives, epoch of the period, the number of TOAs in the timing solution, the MJD range covered by the timing observations, the final rms timing residual and the dispersion measure.

Three of the pulsars in Tables 4 and 5 are members of binary systems. As mentioned in Section 1, all three of these pulsars have been previously published by Camilo et al. (2001); details are repeated here for completeness. Table 6 gives the binary parameters for these pulsars obtained from the timing solutions. Two of these pulsars are in low-eccentricity orbits, for which the longitude and time of periastron are not well determined. For these pulsars the reference epoch is the time of passage through the ascending node. PSR J1454–5846 has a larger (although still small)

Table 3. Flux density calibration pulsars.

PSR J	DM cm^{-3} pc	S_{1400} mJy
1157−6224	325.2	10
1224−6407	97.8	5
1243−6423	297.2	13
1306−6617	436.9	3.9
1326−5859	288.1	10
1327−6222	318.4	12
1327−6301	294.9	3.4
1338−6204	638.0	5.1
1359−6038	294.1	7
1430−6623	65.3	6
1512−5759	628.7	4.0
1522−5829	199.9	4.8
1539−5626	176.5	4.2

---

[5] This page is directly under the multi-beam survey web page given in footnote 1.

Table 4. Positions, flux densities and widths for 100 pulsars discovered in the Parkes multi-beam pulsar survey.

PSR J	RA (J2000) (h m s)	Dec. (J2000) (° ′ ″)	l (°)	b (°)	Beam	Radial Distance	S/N	S_{1400} (mJy)	W_{50} (ms)	W_{10} (ms)
0835−3707	08:35:03.08(3)	−37:07:51.5(3)	257.08	+1.99	2	1.86	20.7	0.28(4)	4.9	12
0838−3947	08:38:30.8(5)	−39:47:22(7)	259.61	+0.93	6	0.86	11.5	0.11(2)	57	–
0901−4624	09:01:40.12(3)	−46:24:48.5(5)	267.40	−0.00	11	1.52	9.6	0.46(6)	5.1	36
0922−4949	09:22:14.96(1)	−49:49:12.08(8)	272.24	+0.16	9	1.04	58.5	0.52(6)	6.9	31
0940−5428	09:40:58.22(4)	−54:28:40.6(3)	277.51	−1.29	12	0.93	33.3	0.35(4)	9.6	–
0954−5430	09:54:06.04(3)	−54:30:53.5(7)	279.00	−0.10	6	0.90	60.9	0.36(5)	7.5	20
0957−5432	09:57:56.01(3)	−54:32:03.9(5)	279.45	+0.23	5	0.62	20.0	0.18(3)	3.6	8
1001−5559	10:01:08.60(3)	−55:59:00.2(3)	280.69	−0.65	8	1.63	14.2	0.64(7)	17.0	59
1002−5559	10:02:57.9(3)	−55:59:37(5)	280.90	−0.50	7	0.82	11.4	0.12(2)	25	–
1016−5819	10:16:12.10(2)	−58:19:01.15(8)	283.71	−1.36	7	1.14	15.9	0.31(4)	4.2	–
1049−5833	10:49:50.34(9)	−58:33:45(1)	287.63	+0.65	12	0.45	53.0	0.72(8)	33	59
1056−5709	10:56:43.8(1)	−57:09:34(1)	287.84	+2.31	10	0.62	11.7	0.11(2)	16.0	–
1112−6103	11:12:14.81(4)	−61:03:31.1(6)	291.22	−0.46	13	0.47	42.7	1.40(15)	11.0	–
1115−6052	11:15:53.68(3)	−60:52:17.8(5)	291.56	−0.13	11	0.46	28.7	0.38(5)	5.4	10
1119−6127	11:19:14.30(2)	−61:27:49.5(2)	292.15	−0.54	3	1.41	33.8	0.90(9)	24	48
1123−6102	11:23:41.70(6)	−61:02:06.2(3)	292.51	+0.05	3	1.46	16.7	0.53(6)	10.0	25
1130−5925	11:30:10.4(1)	−59:25:34.1(7)	292.75	+1.83	4	0.43	17.2	0.12(2)	16.0	–
1138−6207	11:38:21.62(3)	−62:07:59.3(3)	294.51	−0.46	1	0.82	23.0	0.49(6)	12.0	–
1142−6230	11:42:52.5(3)	−62:30:04(1)	295.11	−0.68	12	0.68	15.8	0.26(4)	30	–
1144−6146	11:44:34.8(3)	−61:46:49(3)	295.12	+0.07	11	0.57	63.3	0.45(6)	33	–
1144−6217	11:44:02.11(5)	−62:17:30.3(4)	295.19	−0.44	4	0.57	30.4	0.20(3)	10.0	27
1216−6223	12:16:41.9(1)	−62:23:57.8(9)	298.92	+0.20	1	0.54	13.2	0.15(3)	15.0	–
1220−6318	12:20:17.9(1)	−63:18:46(1)	299.44	−0.65	10	0.68	32.0	0.68(8)	58	–
1224−6208	12:24:44.25(8)	−62:08:41.1(7)	299.82	+0.57	12	0.97	16.2	0.23(3)	10.0	21
1232−6501	12:32:17.840(5)	−65:01:03.33(4)	300.91	−2.22	7	0.51	23.6	0.34(4)	11.0	14
1245−6238	12:45:21.1(1)	−62:38:55.9(8)	302.23	+0.21	9	0.18	16.2	0.14(2)	62	–
1252−6314	12:52:42.6(1)	−63:14:32.7(6)	303.08	−0.37	8	1.89	24.9	0.66(8)	20	41
1301−6305	13:01:45.8(1)	−63:05:34(1)	304.10	−0.24	8	0.21	18.6	0.46(6)	28	–
1303−6305	13:03:00.0(2)	−63:05:01(1)	304.24	−0.24	13	0.96	26.6	0.36(5)	38	78
1305−6203	13:05:20.9(3)	−62:03:22(1)	304.56	+0.77	12	0.78	31.2	0.62(7)	16.0	–
1305−6256	13:05:28.0(4)	−62:56:39(3)	304.53	−0.12	2	1.24	17.0	0.32(4)	19.0	–
1307−6318	13:07:54.7(6)	−63:18:35(4)	304.78	−0.50	10	1.54	29.4	1.40(15)	505	–
1309−6415	13:09:16.6(7)	−64:15:59(5)	304.87	−1.46	2	0.72	16.3	0.21(3)	26	–
1312−6400	13:12:07.2(1)	−64:00:55.6(9)	305.20	−1.23	3	0.45	59.4	0.75(8)	34	61
1317−6302	13:17:44.69(7)	−63:02:52.2(6)	305.91	−0.33	11	0.78	47.1	0.99(11)	12.0	–
1322−6241	13:22:32.1(1)	−62:41:53.5(8)	306.49	−0.04	3	1.49	29.6	0.37(5)	8.7	19
1327−6400	13:27:10.3(1)	−64:00:13.1(6)	306.84	−1.40	3	0.57	29.1	0.36(5)	13.0	120
1341−6023	13:41:07.37(3)	−60:23:34.7(5)	309.04	+1.89	1	1.64	90.4	0.63(7)	9.2	19
1345−6115	13:45:44.4(2)	−61:15:31(2)	309.41	+0.93	3	1.00	51.0	0.59(7)	27	40
1347−5947	13:47:19.38(4)	−59:47:39.8(5)	309.91	+2.32	11	1.09	31.4	0.67(8)	11.0	19
1348−6307	13:48:42.4(4)	−63:07:04(4)	309.35	−0.96	2	1.10	17.5	0.51(6)	79	–
1349−6130	13:49:36.65(4)	−61:30:17.1(4)	309.81	+0.59	5	1.62	13.6	0.58(7)	6.2	14
1406−6121	14:06:50.04(6)	−61:21:27.9(6)	311.84	+0.20	9	0.50	17.1	0.36(5)	16.0	–
1407−6048	14:07:58.6(1)	−60:48:59(1)	312.13	+0.68	7	0.98	13.2	0.20(3)	21	–
1407−6153	14:07:56.5(5)	−61:53:59(6)	311.81	−0.35	1	0.50	16.2	0.36(5)	57	–
1412−6111	14:12:59.6(1)	−61:11:30.5(7)	312.60	+0.14	3	1.03	27.8	0.44(5)	12.0	22
1412−6145	14:12:07.69(5)	−61:45:28.8(6)	312.32	−0.37	2	0.50	30.4	0.47(6)	12.0	–
1413−6222	14:13:05.47(8)	−62:22:28(1)	312.24	−0.99	10	0.62	50.7	0.96(11)	23	–
1416−6037	14:16:30.6(2)	−60:37:59.5(9)	313.18	+0.53	10	0.34	63.1	0.70(8)	13.0	20
1425−6210	14:25:07.7(3)	−62:10:05(1)	313.63	−1.26	13	1.16	10.6	0.19(3)	11.0	–
1429−5935	14:29:25.9(1)	−59:35:59(1)	315.05	+0.95	2	0.58	12.8	0.11(2)	14.0	–
1434−6029	14:34:39.1(3)	−60:29:49(3)	315.31	−0.13	12	0.60	11.0	0.14(2)	19.0	–
1435−6100	14:35:20.2765(4)	−61:00:57.956(6)	315.19	−0.64	8	1.25	12.1	0.25(4)	1.10	–
1444−5941	14:44:46.5(3)	−59:41:19(3)	316.79	+0.10	2	0.88	13.1	0.42(5)	47	79
1452−5851	14:52:52.58(7)	−58:51:13(2)	318.09	+0.40	11	0.52	19.5	0.24(3)	11.0	–
1454−5846	14:54:10.908(2)	−58:46:34.74(3)	318.27	+0.39	13	0.33	12.5	0.24(3)	2.9	5
1513−5739	15:13:58.99(9)	−57:39:01(1)	321.10	+0.10	8	1.28	20.4	0.77(9)	21	33
1530−5327	15:30:26.87(6)	−53:27:56.3(7)	325.33	+2.35	2	1.17	30.0	0.59(7)	14.0	–
1536−5433	15:36:04.8(2)	−54:33:15(4)	325.37	+0.98	11	1.83	40.5	1.30(14)	36	66

Table 4 – *continued*

PSR J	RA (J2000) (h m s)	Dec. (J2000) (° ′ ″)	l (°)	b (°)	Beam	Radial Distance	S/N	S_{1400} (mJy)	W_{50} (ms)	W_{10} (ms)
1537−5645	15:37:51.0(3)	−56:45:04(7)	324.28	−0.94	11	0.68	26.4	1.00(11)	67	–
1538−5438	15:38:49.0(2)	−54:38:17(3)	325.64	+0.68	6	0.79	9.6	0.24(3)	11.0	–
1540−5736	15:40:59.0(1)	−57:36:57(3)	324.11	−1.89	12	0.98	13.9	0.24(3)	14.0	27
1543−5459	15:43:56.25(7)	−54:59:14(1)	326.02	−0.04	12	0.72	28.4	0.62(7)	15.0	37
1548−5607	15:48:44.03(3)	−56:07:33.9(5)	325.86	−1.36	11	0.31	60.2	1.00(11)	7.5	19
1558−5419	15:58:41.5(2)	−54:19:26(5)	328.10	−0.87	7	0.93	18.9	0.40(5)	22	–
1601−5244	16:01:27.3(3)	−52:44:09(3)	329.45	+0.07	1	0.62	14.8	0.13(2)	62	–
1601−5335	16:01:54.91(6)	−53:35:43(1)	328.94	−0.63	9	0.77	16.9	0.22(3)	7.4	–
1605−5215	16:05:19.0(4)	−52:15:48(5)	330.20	+0.03	9	1.10	11.1	0.22(3)	26	–
1607−5140	16:07:49.3(3)	−51:40:16(4)	330.88	+0.21	4	0.67	11.3	0.26(4)	20	–
1609−5158	16:09:26.7(5)	−51:58:18(9)	330.87	−0.18	1	0.71	12.1	0.27(4)	100	–
1610−5006	16:10:44.30(9)	−50:06:42(2)	332.28	+1.05	4	1.55	15.5	1.60(17)	42	98
1611−4949	16:11:46.6(1)	−49:49:57(1)	332.59	+1.14	3	1.23	18.9	0.58(7)	18.0	–
1613−5211	16:13:42.5(1)	−52:11:21(2)	331.20	−0.78	8	0.97	15.5	0.29(4)	14.0	–
1613−5234	16:13:57.5(2)	−52:34:17(3)	330.96	−1.09	13	0.67	13.9	0.28(4)	31	–
1616−5109	16:16:30.9(5)	−51:09:17(9)	332.23	−0.34	2	0.55	32.8	1.20(13)	220	–
1616−5208	16:16:23.4(4)	−52:08:48(4)	331.52	−1.04	8	1.02	17.6	0.44(5)	43	–
1621−5039	16:21:04.7(2)	−50:39:49(2)	333.08	−0.49	3	1.46	11.9	0.36(5)	20	42
1622−4802	16:22:47.2(1)	−48:02:13(1)	335.14	+1.17	4	0.87	38.5	0.92(10)	17.0	–
1622−4944	16:22:37.5(3)	−49:44:30(3)	333.91	−0.01	5	0.38	32.7	0.52(6)	34	–
1623−4949	16:23:54.8(2)	−49:49:04(3)	334.00	−0.21	10	1.53	13.0	0.36(5)	11.0	31
1625−4904	16:25:18.1(1)	−49:04:34(2)	334.69	+0.14	7	0.53	18.6	0.20(3)	13.0	–
1626−4807	16:26:42.5(3)	−48:07:54(4)	335.53	+0.64	3	0.82	11.2	0.37(5)	57	–
1628−4804	16:28:26.8(1)	−48:04:59(3)	335.77	+0.46	3	0.57	58.4	1.00(11)	43	255
1632−4621	16:32:49.81(2)	−46:21:48.6(9)	337.53	+1.10	7	0.94	55.7	0.90(10)	18.0	35
1632−4818	16:32:40.0(2)	−48:18:49(6)	336.08	−0.21	11	0.31	20.4	0.39(5)	43	–
1649−4349	16:49:20.42(8)	−43:49:22(1)	341.36	+0.60	2	1.56	30.0	0.75(8)	26	–
1649−4729	16:49:18.3(1)	−47:29:53(5)	338.54	−1.76	3	0.93	11.8	0.29(4)	18.0	–
1650−4502	16:50:32.30(6)	−45:02:37(2)	340.56	−0.35	12	0.69	26.6	0.35(4)	7.3	19
1653−4249	16:53:40.22(5)	−42:49:03(1)	342.64	+0.63	6	1.63	26.4	1.30(14)	14.0	29
1709−3841	17:09:16.0(2)	−38:41:17(10)	347.71	+0.83	9	0.65	24.0	0.31(4)	19.0	–
1715−3700	17:15:09.7(2)	−37:00:04(14)	349.76	+0.89	6	0.73	14.8	0.37(5)	110	–
1716−3720	17:16:11.36(6)	−37:20:44(3)	349.60	+0.52	12	0.73	29.0	0.41(5)	14.0	105
1718−3825	17:18:13.565(4)	−38:25:18.1(2)	348.95	−0.43	7	1.45	14.4	1.30(14)	3.9	14
1720−3659	17:20:01.976(9)	−36:59:06.5(4)	350.33	+0.10	12	1.43	14.1	0.74(8)	7.5	17
1723−3659	17:23:07.580(6)	−36:59:13.9(3)	350.68	−0.41	7	0.12	113.7	1.50(16)	7.8	35
1724−3505	17:24:47.9(2)	−35:05:36(7)	352.44	+0.38	3	1.21	10.0	0.24(3)	24	–
1725−3546	17:25:42.2(3)	−35:46:16(7)	351.98	−0.15	11	0.50	30.0	0.61(7)	33	–
1726−3530	17:26:07.6(4)	−35:30:05(15)	352.25	−0.07	3	0.73	18.0	0.30(4)	55	–
1726−3635	17:26:49.61(3)	−36:35:46(1)	351.42	−0.80	3	0.46	21.8	0.29(4)	7.8	66
1728−3733	17:28:46.2(2)	−37:33:08(9)	350.84	−1.66	11	0.61	19.9	0.19(3)	8.1	18

eccentricity and the longitude and epoch of periastron could be determined with precision.

Mean pulse profiles at 1374 MHz for the 100 pulsars are given in Fig. 4. As mentioned in Section 3, these profiles were formed by adding all data used for the timing solution. They typically have several hours of effective integration time. For display purposes, these profiles have been corrected for the effects of the high-pass filter in the digitizer. To apply this correction, the profile is first given zero mean. The corrected profile b_n, where n is the bin number and N is the number of bins in the profile, is then given by

$$b_n = a_n, \quad (n = 0)$$

$$b_n = a_n + (t_{bin}/\tau_{HP}) \sum_{m=0}^{n-1} a_m - 1, \quad (0 < n < N) \qquad (15)$$

where a_n is the uncorrected zero-mean profile, t_{bin} is the length of each profile bin in seconds and τ_{HP} is the high-pass filter time constant in seconds. The value of $\tau_{HP} = 0.9\,\text{s}$ was empirically determined by requiring a flat corrected baseline on several long-period pulsars.

Prior to the commencement of the Parkes multi-beam survey, there were 731 known radio pulsars, of which 693 are in the Galactic disc. (Five are in the Magellanic Clouds and 33 are in globular clusters.) Of the 693 disc pulsars, 247 lie within the nominal search area of the multi-beam survey. As the current survey is much more sensitive than any previous survey of this region, we would expect to redetect essentially all of these pulsars. Because of the current incompleteness of the survey, a definitive list of detected previously known pulsars is deferred to a later paper.

Table 5. Period parameters and dispersion measures for 100 pulsars discovered in the Parkes multi-beam pulsar survey.

PSR J	Period, P (s)	$\dot{P}$ (10^{-15})	Epoch (MJD)	N_{toa}	Data span (MJD)	Residual (μs)	DM (cm^{-3} pc)
0835−3707	0.541404373627(15)	9.778(9)	51137.0	27	50940−51333	218	112.3(3)
0838−3947	1.7039457055(9)	0.8(4)	51162.0	19	50941−51382	6149	219(11)
0901−4624	0.441995130786(14)	87.494(8)	51031.0	20	50849−51212	90	198.8(3)
0922−4949	0.950288537028(8)	97.569(4)	51279.0	36	51086−51471	203	237.1(3)
0940−5428	0.087545204308(4)	32.8683(10)	51091.0	38	50849−51333	1027	134.5(9)
0954−5430	0.472834279266(16)	43.912(12)	51034.0	26	50849−51219	185	200.3(4)
0957−5432	0.203556697536(6)	1.947(4)	51035.0	24	50849−51219	126	226.1(3)
1001−5559	1.66117674023(4)	0.860(4)	51172.0	36	50852−51490	511	159.3(9)
1002−5559	0.7775009067(3)	1.57(19)	51035.0	17	50849−51219	490	426(4)
1016−5819	0.0878341561432(9)	0.6980(4)	51155.0	30	50940−51370	124	252.1(4)
1049−5833	2.2023250770(3)	4.41(15)	51031.0	16	50849−51212	1080	446.8(15)
1056−5709	0.67608189374(8)	0.576(14)	51216.0	26	50940−51490	513	436.5(18)
1112−6103	0.064961851894(3)	31.4596(13)	51055.0	45	50849−51261	785	599.1(7)
1115−6052	0.259776659501(9)	7.235(5)	51031.0	24	50849−51212	156	228.2(4)
1119−6127	0.40774589995(5)	4021.782(9)	51485.0	15	51391−51578	137	707(2)
1123−6102	0.64023374765(3)	6.460(8)	51155.0	30	50940−51370	209	439.4(4)
1130−5925	0.68098383242(6)	0.952(7)	51172.0	34	50851−51491	586	264.4(16)
1138−6207	0.117563794023(3)	12.4784(5)	51171.0	39	50849−51491	488	519.8(8)
1142−6230	0.55838338569(10)	0.08(4)	51137.0	16	50940−51334	347	343.8(17)
1144−6146	0.98778306934(16)	−0.04(9)	51032.0	11	50851−51211	233	78.7(13)
1144−6217	0.85066494337(4)	30.835(7)	51110.0	28	50849−51370	439	284.7(6)
1216−6223	0.37404678583(5)	16.819(7)	51111.0	22	50851−51369	224	786.6(18)
1220−6318	0.78921201205(8)	0.080(12)	51216.0	25	50940−51491	1151	347(3)
1224−6208	0.58576120812(4)	20.196(11)	51111.0	24	50851−51369	312	454.2(7)
1232−6501	0.0882819082341(3)	0.00081(2)	51270.0	72	50940−51856	200	239.4(5)
1245−6238	2.2830933508(3)	10.92(5)	51206.0	21	50941−51470	955	336(2)
1252−6314	0.82333927128(6)	0.11(3)	51155.0	25	50940−51369	675	278.4(13)
1301−6305	0.18452809509(6)	266.747(3)	51206.0	37	50940−51471	1540	374(3)
1303−6305	2.3066415539(4)	2.18(16)	51138.0	16	50940−51335	475	343(3)
1305−6203	0.42776184224(8)	32.14(3)	51138.0	17	50940−51335	230	470.0(15)
1305−6256	0.47823093284(12)	2.11(4)	51138.0	15	50941−51335	202	967(3)
1307−6318	4.9624272525(20)	21.1(4)	51206.0	20	50940−51471	4348	374(8)
1309−6415	0.6194535568(3)	8.79(12)	51303.0	15	51087−51517	184	574(5)
1312−6400	2.43743249609(11)	0.68(5)	51303.0	26	51087−51522	974	93.0(12)
1317−6302	0.26127055606(3)	0.102(6)	51138.0	23	50940−51335	205	678.1(12)
1322−6241	0.50605841373(5)	2.587(18)	51138.0	18	50940−51335	298	618.8(19)
1327−6400	0.280677974168(13)	31.177(4)	51206.0	24	50940−51471	703	680.9(14)
1341−6023	0.627285365870(16)	19.461(8)	51280.0	17	51088−51471	210	364.6(9)
1345−6115	1.25308459010(18)	3.25(8)	51138.0	17	50940−51335	366	278(2)
1347−5947	0.609961754304(15)	14.160(7)	51294.0	14	51088−51500	252	293.4(5)
1348−6307	0.9277722389(3)	3.79(7)	51304.0	19	51088−51522	1039	597(3)
1349−6130	0.259362860073(9)	5.125(4)	51138.0	23	50940−51335	123	284.6(4)
1406−6121	0.213074653776(14)	54.701(3)	51111.0	30	50851−51370	1267	542.3(18)
1407−6048	0.49234420664(5)	3.156(8)	51161.0	23	50849−51471	926	575.2(17)
1407−6153	0.7016149492(3)	8.85(7)	51093.0	17	50851−51333	2588	645(9)
1412−6111	0.52915639797(4)	1.91(3)	51031.0	20	50849−51212	265	311.8(9)
1412−6145	0.315224970657(12)	98.6598(13)	51186.0	40	50849−51522	612	514.7(11)
1413−6222	0.29240770249(3)	2.229(6)	51092.0	27	50849−51333	368	808.1(12)
1416−6037	0.29558048193(3)	4.280(15)	51031.0	18	50849−51212	169	289.2(10)
1425−6210	0.50173030987(8)	0.48(4)	51031.0	15	50849−51212	256	430.1(17)
1429−5935	0.76391483053(8)	42.751(9)	51232.0	21	50940−51523	550	457(2)
1434−6029	0.96334832315(16)	1.03(8)	51137.0	16	50940−51333	407	282(3)
1435−6100	0.009347972210248(6)	0.0000245(4)	51270.0	93	50939−51856	14	113.7(6)
1444−5941	2.7602279448(6)	8.2(3)	51137.0	17	50941−51333	746	177.1(19)
1452−5851	0.38662501748(3)	50.706(18)	51280.0	16	51088−51472	146	262.4(15)
1454−5846	0.04524777299802(9)	0.000816(7)	51300.0	81	50981−51856	100	115.95(16)
1513−5739	0.97345803480(9)	27.55(4)	51137.0	20	50941−51333	480	469.7(10)
1530−5327	0.278956721152(15)	4.683(4)	51253.0	26	51013−51491	402	49.6(10)
1536−5433	0.8814384311(3)	1.91(8)	51138.0	21	50941−51334	1529	147.5(19)

Table 5 – *continued*

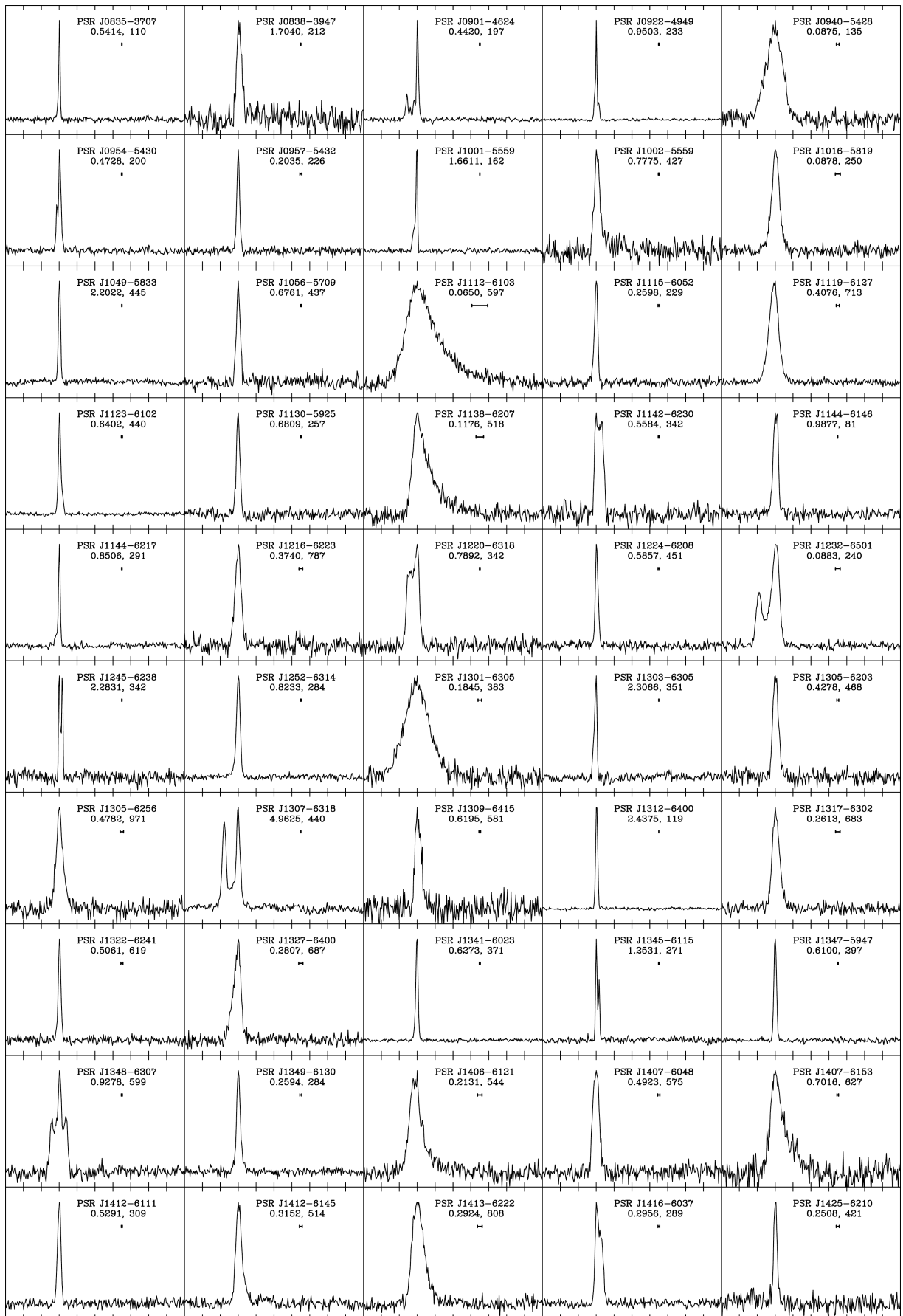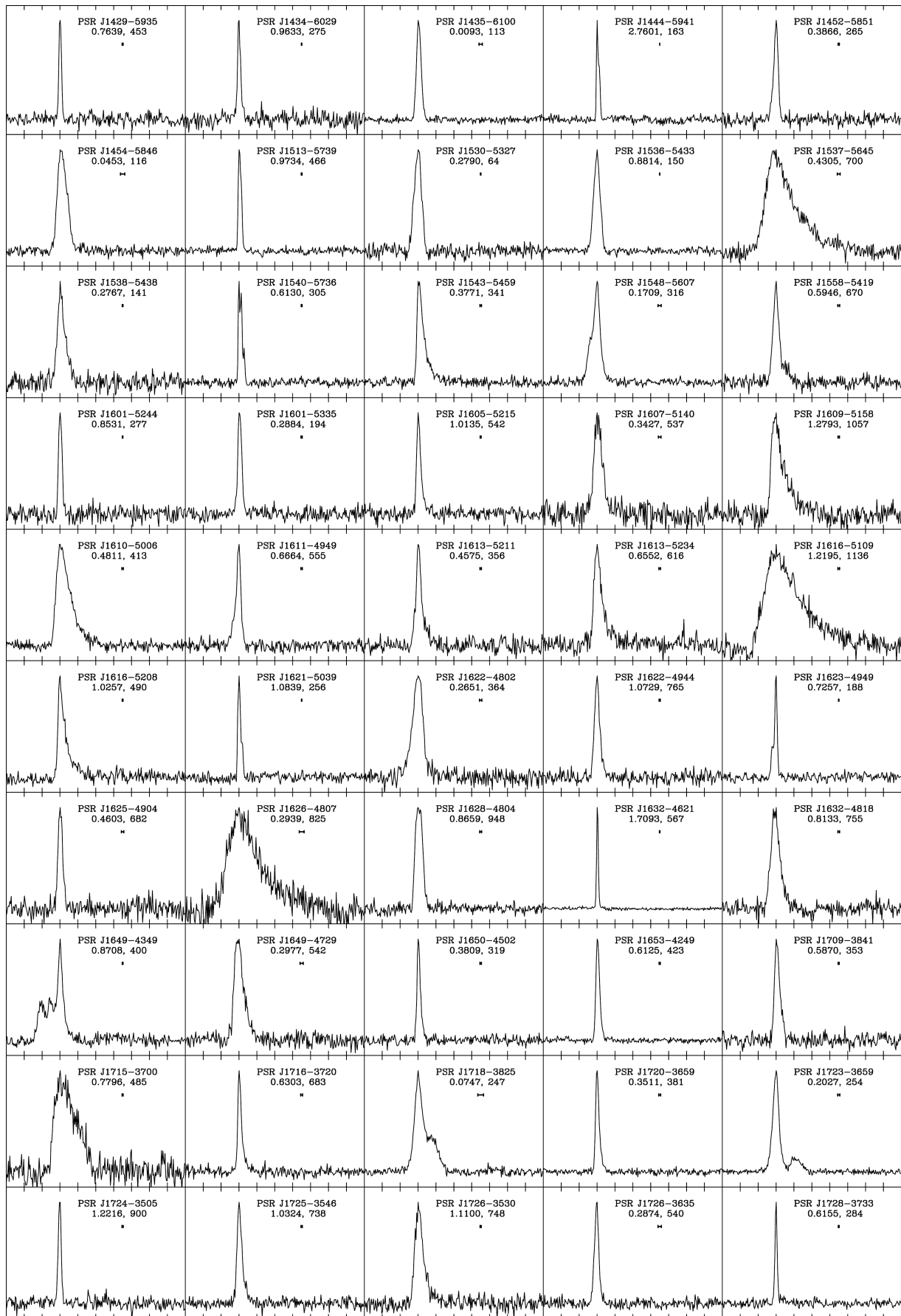| PSR J	Period, P (s)	$\dot{P}$ (10^{-15})	Epoch (MJD)	N_{toa}	Data span (MJD)	Residual (μs)	DM $(cm^{-3}\,pc)$
1537−5645	0.43046412386(15)	2.78(6)	51306.0	18	51088−51524	830	707(5)
1538−5438	0.27672613726(5)	1.42(3)	51138.0	19	50941−51334	885	136.9(17)
1540−5736	0.61291628569(8)	0.42(3)	51309.0	21	51089−51528	482	304.5(13)
1543−5459	0.37711856263(3)	52.018(9)	51139.0	21	50941−51371	253	345.7(10)
1548−5607	0.170933992695(5)	10.736(3)	51138.0	33	50941−51334	220	315.5(4)
1558−5419	0.59457526355(15)	6.04(6)	51138.0	16	50941−51334	480	657(3)
1601−5244	2.559356631(7)	0.72(14)	51071.0	17	50849−51292	726	273(3)
1601−5335	0.288456511543(16)	62.371(6)	51156.0	26	50941−51371	462	194.6(7)
1605−5215	1.0136087473(5)	4.75(11)	51072.0	20	50851−51292	6570	532(4)
1607−5140	0.34272279247(9)	2.54(4)	51072.0	20	50849−51293	2204	533(3)
1609−5158	1.2794023539(7)	12.96(10)	51160.0	23	50849−51470	3299	1069(8)
1610−5006	0.48111885215(5)	13.625(10)	51111.0	27	50849−51371	917	416(3)
1611−4949	0.66643792285(8)	0.54(3)	51071.0	22	50849−51292	546	556.8(18)
1613−5211	0.45750181782(7)	19.231(17)	51072.0	16	50849−51293	259	360(2)
1613−5234	0.65522059567(18)	6.629(18)	51111.0	22	50849−51463	501	624(4)
1616−5109	1.2195938825(8)	19.08(9)	51161.0	24	50849−51471	3230	1160(15)
1616−5208	1.0258308926(4)	28.91(10)	51072.0	16	50849−51293	688	488(3)
1621−5039	1.08401994353(16)	13.03(5)	51072.0	20	50849−51293	642	261(3)
1622−4802	0.26507223569(3)	0.307(15)	51033.0	17	50851−51213	160	364.3(13)
1622−4944	1.0729678942(3)	17.08(7)	51072.0	21	50849−51293	1711	755(4)
1623−4949	0.72573215540(9)	42.09(4)	51073.0	21	50851−51293	374	183.3(10)
1625−4904	0.46033949229(7)	16.76(2)	51073.0	17	50852−51293	275	684.8(17)
1626−4807	0.29392818864(7)	17.476(12)	51207.0	23	50941−51472	5286	817(6)
1628−4804	0.86597096270(12)	1.24(4)	51073.0	20	50851−51293	643	952(3)
1632−4621	1.70915449528(4)	76.02(3)	51291.0	18	51089−51492	340	562.9(8)
1632−4818	0.81342978867(20)	650.64(4)	51112.0	23	50852−51371	1439	758(5)
1649−4349	0.87071155949(7)	0.044(19)	51243.0	19	51013−51472	402	398.6(12)
1649−4729	0.29769219971(5)	6.550(16)	51157.0	19	50941−51371	1280	540.2(18)
1650−4502	0.38086979928(5)	16.061(16)	51118.0	15	50941−51294	228	319.7(8)
1653−4249	0.61255824122(5)	4.81(3)	51118.0	18	50940−51294	192	416.1(11)
1709−3841	0.58698616319(18)	7.86(11)	51117.0	17	50941−51292	995	356(3)
1715−3700	0.7796281140(4)	0.15(5)	51118.0	23	50852−51383	2975	449(11)
1716−3720	0.63031371285(6)	17.970(12)	51112.0	25	50852−51371	418	682.7(17)
1718−3825	0.0746699205656(4)	13.22167(7)	51184.0	37	50877−51490	52	247.4(3)
1720−3659	0.351124633722(5)	0.0327(9)	51111.0	30	50851−51369	162	381.6(5)
1723−3659	0.2027219378604(17)	8.0075(4)	51118.0	25	50851−51383	129	254.2(3)
1724−3505	1.2217076921(3)	21.10(9)	51074.0	20	50852−51294	1251	875(3)
1725−3546	1.0324711993(4)	15.00(8)	51074.0	17	50852−51294	2137	744(4)
1726−3530	1.1100937711(12)	1217.94(5)	51154.0	27	50852−51455	2577	727(7)
1726−3635	0.287431567184(13)	1.440(3)	51111.0	22	50852−51369	153	539.2(7)
1728−3733	0.61553824309(16)	0.07(4)	51112.0	19	50852−51370	257	281.5(7)

5   DISCUSSION AND CONCLUSIONS

In this paper we have described in some detail the Parkes multi-beam pulsar survey, currently being conducted using a 13-beam receiver operating at a central frequency of 1374 MHz on the Parkes 64-m radio telescope. Data acquisition and analysis techniques are described and a detailed discussion of the survey sensitivity and observing strategy is given. After confirmation of a candidate, timing data are obtained, typically over a 12–18 month period, giving an accurate position, pulse period, period derivative and DM. The pulse width and mean flux density are estimated from the mean pulse profile. We give the principal observed properties of the first 100 pulsars discovered in the survey.

Table 7 gives derived parameters for these 100 pulsars. After the name, the first three columns give the $\log_{10}$ of the characteristic age, $\tau_c = P/(2\dot{P})$ (in years), the surface dipole magnetic field, $B_s = 3.2 \times 10^{19}(P\dot{P})^{1/2}$ (in gauss), and the rate of loss of rotational energy, $\dot{E} = 4\pi^2 I\dot{P}P^{-3}$ (in erg s^{-1}), where a neutron-star moment of inertia $I = 10^{45}$ g cm^2 is assumed. The next two columns give the pulsar distance, d, computed from the DM assuming the Taylor & Cordes (1993) model for the Galactic distribution of free electrons, and the implied Galactic z-distance. Although distances are quoted to 0.1 kpc, in fact they are generally more uncertain than that owing to uncertainties in the electron density model. This is especially so for pulsars with very large DMs, indicating large distances from the Sun. The final column gives the radio luminosity $L_{1400} = S_{1400}d^2$. Pulsars discovered at relatively high radio frequencies, for example, at 1400 MHz, tend to have a flatter spectrum than those discovered at lower frequencies. For example, the sample of pulsars discovered by Johnston et al. (1992) has a

PSR J0835−3707
0.5414, 110

PSR J0838−3947
1.7040, 212

PSR J0901−4624
0.4420, 197

PSR J0922−4949
0.9503, 233

PSR J0940−5428
0.0875, 135

PSR J0954−5430
0.4728, 200

PSR J0957−5432
0.2035, 226

PSR J1001−5559
1.6611, 162

PSR J1002−5559
0.7775, 427

PSR J1016−5819
0.0878, 250

PSR J1049−5833
2.2022, 445

PSR J1056−5709
0.6761, 437

PSR J1112−6103
0.0650, 597

PSR J1115−6052
0.2598, 229

PSR J1119−6127
0.4076, 713

PSR J1123−6102
0.6402, 440

PSR J1130−5925
0.6809, 257

PSR J1138−6207
0.1176, 518

PSR J1142−6230
0.5584, 342

PSR J1144−6146
0.9877, 81

PSR J1144−6217
0.8506, 291

PSR J1216−6223
0.3740, 787

PSR J1220−6318
0.7892, 342

PSR J1224−6208
0.5857, 451

PSR J1232−6501
0.0883, 240

PSR J1245−6238
2.2831, 342

PSR J1252−6314
0.8233, 284

PSR J1301−6305
0.1845, 383

PSR J1303−6305
2.3066, 351

PSR J1305−6203
0.4278, 468

PSR J1305−6256
0.4782, 971

PSR J1307−6318
4.9625, 440

PSR J1309−6415
0.6195, 581

PSR J1312−6400
2.4375, 119

PSR J1317−6302
0.2613, 683

PSR J1322−6241
0.5061, 619

PSR J1327−6400
0.2807, 687

PSR J1341−6023
0.6273, 371

PSR J1345−6115
1.2531, 271

PSR J1347−5947
0.6100, 297

PSR J1348−6307
0.9278, 599

PSR J1349−6130
0.2594, 284

PSR J1406−6121
0.2131, 544

PSR J1407−6048
0.4923, 575

PSR J1407−6153
0.7016, 627

PSR J1412−6111
0.5291, 309

PSR J1412−6145
0.3152, 514

PSR J1413−6222
0.2924, 808

PSR J1416−6037
0.2956, 289

PSR J1425−6210
0.2508, 421

Table 6. Binary pulsar parameters (Camilo et al. 2001).

	PSR J1232 − 6501	PSR J1435 − 6100	PSR J1454 − 5846
Orbital period (d)	1.86327241(8)	1.354 885 217(2)	12.423 065 5(2)
Projected semi-major axis (s)	1.61402(6)	6.184 023(4)	26.528 90(4)
Eccentricity	0.00011(8)	0.000010(2)	0.001 898(3)
Longitude of periastron (deg)	129(45)	10(6)	310.1(1)
Epoch of ascending node (MJD)	51269.98417(2)	51 270.608 444 9(5)	51 303.833(4)*

  * Epoch of periastron.

mean spectral index of −1.0 compared to the value of −1.7 found for pulsars detected in the Parkes 70-cm survey (Toscano et al. 1998). However, the Johnston et al. and Clifton et al. surveys were the first extensive surveys at these higher frequencies. Most of the previously discovered pulsars had been found in lower-frequency searches, which selected the steeper-spectrum pulsars. The present survey is much more sensitive than any previous survey of this region, and hence the discovered pulsars are a largely unbiased sample. Adopting a compromize mean spectral index of −1.3 for the multi-beam discoveries, the L_{1400} values may be converted to the more commonly quoted 400-MHz luminosity by multiplying by 5.0.

Fig. 5 gives histograms of the distributions in pulse period for the 100 multi-beam pulsars and previously known disc pulsars, i.e. excluding those in globular clusters and the Magellanic Clouds. For the so-called 'normal' or non-millisecond pulsars, the distribution of the multi-beam pulsars is similar to that of previously known pulsars, except for a larger number of pulsars with periods of just less than 100 ms. As shown by Table 7, three of these, PSRs J0940–5428, J1112–6103 and J1718–3825, are relatively young pulsars with ages between 30 000 and 100 000 years and spin-down luminosities in excess of 10^{36} erg s^{-1}. The other two, PSRs J1232–6501 and J1454–5846, have very small period derivatives and are members of binary systems (Table 6). As discussed by Camilo et al. (2001), both of these systems have unusual properties. The first is atypical of low-mass binary pulsars, having a relatively long spin period, while the second is unusual in that it has a larger companion mass and higher eccentricity than most pulsar–white-dwarf binaries. 11 of these first 100 pulsars have characteristic ages of less than 100 kyr; this is a much higher proportion than that for the previously known population.

Only one millisecond pulsar, PSR J1435–6100, which has a period of 9.3 ms and is a member of a binary system (Table 6), is included in first 100 pulsars discovered by the Parkes multi-beam survey (although several more have subsequently been discovered). As Fig. 5 shows, this is a much smaller proportion than that for previously known pulsars, although it is worth noting that there are no previously known disc millisecond pulsars within the area currently searched ($|b| \lesssim 1°.5$). There are several factors which contribute to this low detection rate for millisecond pulsars. This paper reports the earliest multi-beam survey observations which were made along and adjacent to the Galactic equator – the vast majority of the discovered pulsars have Galactic latitudes of $\lesssim 1°$ (Table 4). At these latitudes, the volume searched for millisecond pulsars is greatly reduced by dispersion broadening. Fig. 2 shows

that the sensitivity is halved for a 10-ms pulsar with DM of 100 cm^{-3} pc, corresponding to a distance of 3 kpc or less in the Galactic plane. The generally lower luminosity of millisecond pulsars results in a flux density limited distribution which extends to high Galactic latitudes (Lyne et al. 1998), so the expected number in our search volume is small. Furthermore, most radio-frequency interference produces spurious signals at millisecond periods. At the early stage at which most of these data were processed, techniques for eliminating the effects of interference were not optimized. Consequently, real pulsars tended to be lost in a forest of spurious candidates. Finally, many millisecond pulsars are members of binary systems. The long observation time of this survey tends to discriminate against detection of short-period binary systems. All of these factors have been or will be largely overcome in subsequent observations and analyses.

At the other end of the period range, PSR J1307–6318 has a pulse period of 4.96 s, the third longest known. Unlike PSR J2144–3933, the 8.5-s pulsar (Young et al. 1999), PSR J1307–6318 has a relatively wide double pulse (Fig. 4) with a 50 per cent width of 505 ms, more than 10 per cent of the period.

Fig. 6 shows that the DM distribution of the multi-beam pulsars is very different from that of previously known pulsars, peaking at a DM of 300 cm^{-3} pc or so. This is readily explained by the low Galactic latitude and very high sensitivity of the multi-beam survey. Most of the pulsars are distant and of relatively high luminosity (Table 7). The Taylor & Cordes (1993) distance model puts many of them at distances greater than that of the Galactic Centre, and several are beyond the limit of the model (those with a distance of 30 kpc in Table 7) and certainly over-estimated. Fig. 4 shows that a significant number of these distant pulsars have highly scattered profiles. However, there is not a close relationship between DM and the width of the scattering tail, with several pulsars of similar period and dispersion measure (e.g. PSRs J1609–5158 and J1616–5109) having quite different scattering times (Manchester 2000). We expect that the pulsars discovered in this survey will make a major contribution to improving our knowledge of the Galactic electron density model and the distribution of the fluctuations responsible for interstellar scattering, especially in the central regions of the Galaxy.

Finally, in Fig. 7 we show the distribution of mean 1400-MHz flux densities for the multi-beam pulsars. Of the two-thirds of known pulsars with a published 1400-MHz flux density, only about 10 per cent have a value of less than 1 mJy. Values above 1 mJy are generally only quoted to the nearest mJy, so they are not well suited to be displayed in Fig. 7. About 10 newly discovered pulsars have

Figure 4. Mean pulse profiles for 100 pulsars discovered in the Parkes multi-beam survey. The highest point in the profile is placed at phase 0.3. For each profile, the pulsar name, pulse period (in s) and DM (in cm^{-3} pc) are given. The small horizontal bar under the period indicates the effective resolution of the profile, including the effects of interstellar dispersion.

Table 7. Derived parameters for 100 pulsars discovered in Parkes multi-beam pulsar survey.

PSR J	$\log[\tau_c]$ (yr)	$\log[B_s]$ (G)	$\log[\dot{E}]$ (erg s^{-1})	Distance (kpc)	z (kpc)	L_{1400} (mJy kpc^2)
0835−3707	5.94	12.37	33.38	2.3	+0.08	1.5
0838−3947	7.52	12.08	30.81	8.2	+0.13	7.4
0901−4624	4.90	12.80	34.60	7.5	−0.00	25.6
0922−4949	5.19	12.99	33.65	10.4	+0.03	56.2
0940−5428	4.63	12.24	36.28	4.3	−0.10	6.4
0954−5430	5.23	12.66	34.20	6.2	−0.01	13.8
0957−5432	6.22	11.80	33.96	7.0	+0.03	8.8
1001−5559	7.49	12.08	30.87	3.9	−0.04	9.9
1002−5559	6.89	12.05	32.11	17.4	−0.15	36.3
1016−5819	6.30	11.40	34.61	4.6	−0.11	6.6
1049−5833	6.90	12.50	31.20	9.7	+0.11	68.0
1056−5709	7.27	11.80	31.87	17.6	+0.71	34.1
1112−6103	4.51	12.16	36.65	>30.0	<−0.24	>1260.0
1115−6052	5.76	12.14	34.20	6.8	−0.01	17.4
1119−6127	3.21	13.61	36.36	>30.0	<−0.28	>720.0
1123−6102	6.20	12.31	32.99	14.7	+0.01	114.5
1130−5925	7.05	11.91	32.08	8.3	+0.27	8.2
1138−6207	5.17	12.09	35.48	24.5	−0.20	294.1
1142−6230	8.05	11.32	31.26	10.8	−0.13	30.3
1144−6146	>8.50	<11.35	<31.35	10.8	−0.13	30.3
1144−6217	5.64	12.71	33.30	8.9	−0.07	15.8
1216−6223	5.55	12.40	34.11	>30.0	>+0.10	>135.0
1220−6318	8.19	11.41	30.81	14.0	−0.16	133.3
1224−6208	5.66	12.54	33.60	23.6	+0.23	128.1
1232−6501	9.25	9.93	31.66	10.0	−0.39	30.0
1245−6238	6.52	12.70	31.56	14.6	+0.05	29.8
1252−6314	8.08	11.48	30.89	11.0	−0.07	79.9
1301−6305	4.04	12.85	36.23	15.8	−0.07	114.8
1303−6305	7.22	12.36	30.85	13.6	−0.06	66.6
1305−6203	5.32	12.57	34.20	24.1	+0.32	360.1
1305−6256	6.55	12.01	32.88	>30.0	<−0.06	>288.0
1307−6318	6.57	13.02	30.83	14.4	−0.12	290.3
1309−6415	6.05	12.37	33.18	>30.0	<−0.77	>189.0
1312−6400	7.75	12.12	30.28	2.2	−0.05	3.7
1317−6302	7.61	11.22	32.36	>30.0	<−0.17	>891.0
1322−6241	6.49	12.06	32.90	19.9	−0.01	146.5
1327−6400	5.15	12.48	34.75	>30.0	<−0.73	>324.0
1341−6023	5.71	12.55	33.49	7.0	+0.23	31.1
1345−6115	6.79	12.31	31.81	5.9	+0.10	20.3
1347−5947	5.83	12.47	33.40	6.5	+0.26	28.6
1348−6307	6.59	12.28	32.28	8.2	−0.14	34.1
1349−6130	5.90	12.07	34.08	5.8	+0.06	19.6
1406−6121	4.79	12.54	35.34	9.1	+0.03	29.9
1407−6048	6.39	12.10	33.00	9.7	+0.12	18.8
1407−6153	6.10	12.40	33.00	9.8	−0.06	34.2
1412−6111	6.64	12.01	32.71	6.0	+0.01	15.6
1412−6145	4.70	12.75	35.08	9.3	−0.06	40.8
1413−6222	6.32	11.91	33.54	27.7	−0.48	736.6
1416−6037	6.04	12.06	33.81	5.7	+0.05	22.9
1425−6210	7.22	11.70	32.18	10.0	−0.22	18.9
1429−5935	5.45	12.76	33.58	10.6	+0.18	12.4
1434−6029	7.17	12.00	31.65	5.8	−0.01	4.7
1435−6100	9.81	8.67	33.04	3.2	−0.04	2.1
1444−5941	6.73	12.68	31.18	4.4	+0.01	8.1
1452−5851	5.08	12.65	34.54	5.6	+0.04	7.6
1454−5846	8.95	9.78	32.53	3.3	+0.02	2.2
1513−5739	5.75	12.72	33.08	9.8	+0.02	74.6
1530−5327	5.97	12.06	33.93	1.5	+0.06	1.3

Table 7 – *continued*

PSR J	log[τ_c] (yr)	log[B_s] (G)	log[$\dot{E}$] (erg s^{-1})	Distance (kpc)	z (kpc)	L_{1400} (mJy kpc^2)
1536−5433	6.86	12.12	32.04	3.7	+0.06	18.0
1537−5645	6.39	12.05	33.15	24.7	−0.41	610.1
1538−5438	6.49	11.80	33.43	3.6	+0.04	3.1
1540−5736	7.36	11.71	31.86	8.2	−0.27	16.0
1543−5459	5.06	12.65	34.58	6.3	−0.00	24.8
1548−5607	5.40	12.14	34.93	7.0	−0.17	48.3
1558−5419	6.19	12.28	33.04	9.1	−0.14	33.1
1601−5244	7.75	12.14	30.23	5.1	+0.01	3.4
1601−5335	4.86	12.63	35.00	4.0	−0.04	3.6
1605−5215	6.53	12.35	32.26	7.1	+0.00	11.0
1607−5140	6.33	11.97	33.40	7.0	+0.03	12.8
1609−5158	6.19	12.61	32.38	12.7	−0.04	43.5
1610−5006	5.75	12.41	33.68	6.6	+0.12	69.5
1611−4949	7.29	11.78	31.86	8.8	+0.18	45.1
1613−5211	5.58	12.48	33.90	6.2	−0.08	11.0
1613−5234	6.19	12.32	32.97	9.9	−0.19	27.6
1616−5109	6.01	12.69	32.62	18.9	−0.11	428.7
1616−5208	5.75	12.74	33.04	7.4	−0.13	23.9
1621−5039	6.12	12.58	32.60	4.9	−0.04	8.6
1622−4802	7.14	11.46	32.81	6.0	+0.12	33.1
1622−4944	6.00	12.64	32.74	8.6	−0.00	38.0
1623−4949	5.44	12.75	33.63	3.8	−0.01	5.1
1625−4904	5.64	12.45	33.83	7.9	+0.02	12.6
1626−4807	5.43	12.36	34.43	10.2	+0.11	38.5
1628−4804	7.04	12.02	31.88	11.2	+0.09	125.4
1632−4621	5.55	13.06	32.78	8.4	+0.16	63.8
1632−4818	4.30	13.37	34.68	8.5	−0.03	28.4
1649−4349	8.50	11.30	30.41	5.6	+0.06	23.2
1649−4729	5.86	12.15	33.99	12.7	−0.39	46.8
1650−4502	5.57	12.40	34.04	5.1	−0.03	9.1
1653−4249	6.30	12.24	32.92	5.6	+0.06	41.4
1709−3841	6.07	12.34	33.18	5.2	+0.08	8.3
1715−3700	7.93	11.53	31.08	6.1	+0.09	13.6
1716−3720	5.74	12.53	33.45	9.4	+0.09	36.6
1718−3825	4.95	12.00	36.11	4.2	−0.03	23.4
1720−3659	8.23	11.03	31.48	5.1	+0.01	19.3
1723−3659	5.60	12.11	34.58	4.3	−0.03	27.5
1724−3505	5.96	12.71	32.66	12.0	+0.08	34.6
1725−3546	6.04	12.60	32.73	10.2	−0.03	63.5
1726−3530	4.16	13.57	34.54	10.0	−0.01	29.9
1726−3635	6.50	11.81	33.38	7.4	−0.10	15.8
1728−3733	8.13	11.33	31.08	4.9	−0.14	4.6

$S_{1400} \lesssim 0.2$ mJy, lower than the nominal survey limiting flux density. Interstellar scintillation is not normally observed for the pulsars discovered in this survey, as diffractive scintillation bandwidths are much less than the observed bandwidth of 288 MHz and refractive scintillations are weak for high-DM pulsars (Rickett 1977; Kaspi & Stinebring 1992). The principal reason for the low observed flux densities is the dependence of effective survey sensitivity on pulse width (Section 2.3). With only a few exceptions, observed flux densities are greater than the nominal limiting flux density scaled by $[W_{50}/(P - W_{50})/0.05]^{1/2}$.

Another factor is that many pulsars show intrinsic intensity variations such as nulling, and it is likely that some of these pulsars were detected when they had a greater than average flux density. As expected, most of the detected pulsars are relatively weak, with mean flux densities in the range 0.2 to 0.5 mJy. However, because of the large distances of most of these pulsars, their luminosities are typically large (Table 7). All have $L_{1400} > 1$ mJy kpc^2, corresponding to $L_{400} \gtrsim 5$ mJy kpc^2 and most are above the low-luminosity cut-off in the luminosity distribution which, at 400 MHz, begins at about 10 mJy kpc^2 (Lyne et al. 1998).

The newly discovered pulsars reported in this paper represent only a small fraction of the total sample which will be discovered by the Parkes multi-beam pulsar survey when it is complete. We therefore defer a more detailed analysis of the properties of the multi-beam sample, its relation to previously known pulsars and its
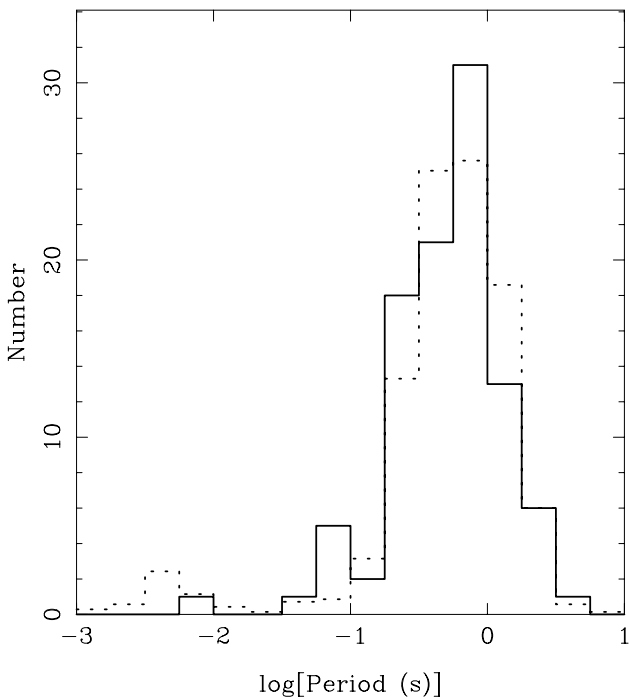
Figure 5. Distribution in period of the 100 Parkes multi-beam pulsars (solid line) and of previously known pulsars (dotted line). For the previously known pulsars, the vertical scale has been adjusted to equalize the number of pulsars in the two distributions.
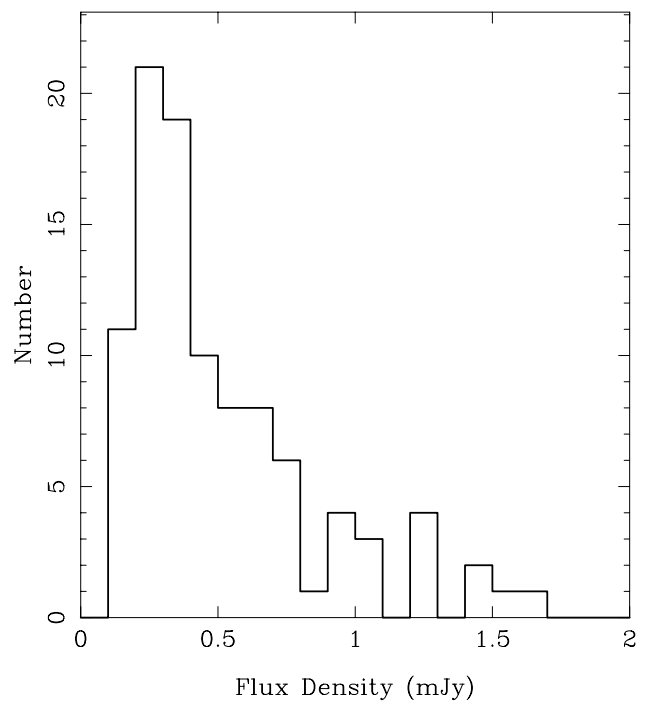
Figure 7. Distribution in mean flux density at 1400 MHz of the 100 Parkes multi-beam pulsars.

implications for the Galactic distribution and evolution of pulsars to later publications.
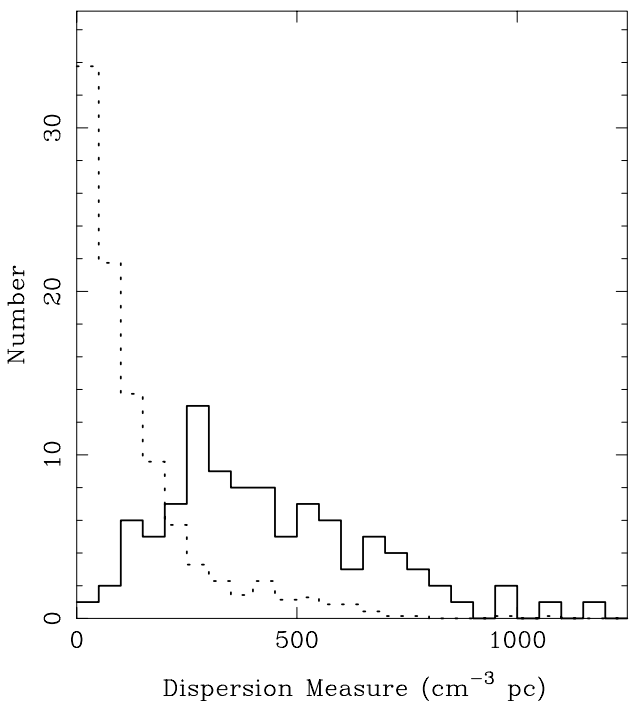
Figure 6. Distribution in DM of the 100 Parkes multi-beam pulsars (solid line) and of previously known pulsars (dotted line). For the previously known pulsars, the vertical scale has been adjusted to equalise the number of pulsars in the two distributions.

REFERENCES

Backer D. C., Kulkarni S. R., Heiles C., Davis M. M., Goss W. M., 1982, Nat, 300, 615

Camilo F. et al., 2000a, in Kramer M., Wex N., Wielebinski R. eds, Proc.

IAU Colloq. 177, Pulsar Astronomy – 2000 and Beyond. Astron. Soc. Pac., San Francisco, p. 3

Camilo F. M., Kaspi V. M., Lyne A. G., Manchester R. N., Bell J. F., D'Amico N., McKay N. P. F., Crawford F., 2000b, ApJ, 541, 367

Camilo F. et al., 2001, ApJ, 548, L187

Clifton T. R., Lyne A. G., Jones A. W., McKenna J., Ashworth M., 1992, MNRAS, 254, 177

Cordes J. M., Chernoff D. F., 1998, ApJ, 505, 315

Crawford F., 2000, PhD thesis Massachusetts Institute of Technology

Crawford F., Gaensler B. M., Kaspi V. M., Manchester R. N., Camilo F., Lyne A. G., Pivovaroff M. J., 2001, ApJ, 554, 152

D'Amico N. et al., 2000, in Palumbo G., White N. eds, Proceedings of X-ray Astronomy 1999: Stellar Endpoints, AGN and the X-ray Background. Gordon & Breach, Singapore, in press

D'Amico N. et al., 2001, ApJ, 552, L45

Fruchter A. S., Stinebring D. R., Taylor J. H., 1988, Nat, 333, 237

Hartman J. W., Bhattacharya D., Wijers R., Verbunt F., 1997, A&A, 322, 477

Haslam C. G. T., Salter C. J., Stoffel H., Wilson W. E., 1982, A&AS, 47, 1

Hewish A., Bell S. J., Pilkington J. D. H., Scott P. F., Collins R. A., 1968, Nat, 217, 709

Hulse R. A., Taylor J. H., 1974, ApJ, 191, L59

Johnston S., Lyne A. G., Manchester R. N., Kniffen D. A., D'Amico N., Lim J., Ashworth M., 1992a, MNRAS, 255, 401

Johnston S., Manchester R. N., Lyne A. G., Bailes M., Kaspi V. M., Qiao G., D'Amico N., 1992b, ApJ, 387, L37

Kaspi V. M., 2000, in Kramer M., Wex N., Wielebinski R. eds, Proc. IAU Colloq. 177, Pulsar Astronomy – 2000 and Beyond. Astron. Soc. Pac., San Francisco, p. 485

Kaspi V. M., Stinebring D. R., 1992, ApJ, 392, 530

Kaspi V. M. et al., 2000, ApJ, 543, 321

Lorimer D. R., Bailes M., Dewey R. J., Harrison P. A., 1993, MNRAS, 263, 403

Lyne A. G., Manchester R. N., Taylor J. H., 1985, MNRAS, 213, 613

Lyne A. G. et al., 1998, MNRAS, 295, 743

Lyne A. G. et al., 2000, MNRAS, 312, 698

Lyne A. G., Shemar S. L., Graham-Smith F., 2000, MNRAS, 315, 534

Manchester R. N., 2000, in Strom R. ed., Proc. IAU Colloq. 182, Sources and Scintillations: refraction and scattering in radio astronomy. Kluwer, Dordrecht in press

Manchester R. N. et al., 1996, MNRAS, 279, 1235

Manchester R. N. et al., 2000, in Kramer M., Wex N., Wielebinski R. eds, Proc. IAU Colloq. 177, Pulsar Astronomy – 2000 and Beyond. Astron. Soc. Pac., San Francisco, p. 49

Navarro J., Manchester R. N., Sandhu J. S., Kulkarni S. R., Bailes M., 1997, ApJ, 486, 1019

Pivovaroff M., Kaspi V. M., Camilo F., 2000, ApJ, 535, 379

Pivovaroff M. J., Kaspi V. M., Camilo F., Gaensler B. M., Crawford F., 2001, ApJ, 554, 161

Rickett B. J., 1977, ARA&A, 15, 479

Shemar S. L., Lyne A. G., 1996, MNRAS, 282, 677

Staelin D. H., Reifenstein E. C., III, 1968, Sci, 162, 1481

Stairs I. H. et al., 2001, MNRAS, 325, 979

Standish E. M., 1990, A&A, 233, 252

Staveley-Smith L. et al., 1996, Proc. Astr. Soc. Aust., 13, 243

Taylor J. H., Cordes J. M., 1993, ApJ, 411, 674

Taylor J. H., Weisberg J. M., 1989, ApJ, 345, 434

Taylor J. H., 1974, A&AS, 15, 367

Taylor J. H., Manchester R. N., Lyne A. G., 1993, ApJS, 88, 529

Thompson D. J. et al., 1999, ApJ, 516, 297

Toscano M., Bailes M., Manchester R., Sandhu J., 1998, ApJ, 506, 863

Van Vleck J. H., Middleton D., 1966, Proc. IEEE, 54, 2

Wallace P. T. et al., 1977, Nat, 266, 692

Wang N., Manchester R. N., Pace R., Bailes M., Kaspi V. M., Stappers B. W., Lyne A. G., 2000, MNRAS, 317, 843

Wolszczan A., Frail D. A., 1992, Nat, 355, 145

Young M. D., Manchester R. N., Johnston S., 1999, Nat, 400, 848

This paper has been typeset from a TEX/LATEX file prepared by the author.